Meandering-like river channel evolution due to the formation of fluvial bars

(砂州の形成によって発生する蛇行状流路変動)

Kristine Domogoy Sanchez

A thesis submitted in partial fulfillment for the degree of Doctor of Engineering

Examination Committee: Prof. Norihiro Izumi
Prof. Yasuyuki Shimizu
Prof. Toshihiko Yamashita

Doctoral Thesis No.

Division of Field Engineering for the Environment
Graduate School of Engineering, Hokkaido University

March 2019

Acknowledgment

I wish to express my sincere gratitude to Prof. Norihiro N. Izumi, whose support helped me with my study. Thank you very much, sensei. Thank you for the lessons learned.

I thank Prof. Tomohito J. Yamada, for the support as well;

To Sir Adriano C. de Lima, Sytharith Pen and Randulph Paulo B. Morales, for the extended assistance on the research work;

To the Filipino students of Hokkaido University, most especially to the Bisaya students, for the encouragement and warm companionship;

To my labmates of the River and Watershed Engineering Laboratory, and the e3 family, for the assistance towards my study and stay in Japan;

Thank you to my family and friends, who are my constant source of motivation;

And to JICA Sapporo and AUN/Seed-Net, for providing an opportunity to be able to study in, and explore Japan. Thank you.

Abstract

Depending upon the fluid flow and sediment transport conditions, a variety of structures can develop on the riverbed whenever perturbations are induced. These include ripples, dunes, antidunes and alternate bars. Among these, alternate bars are megascale bedforms that arise upon the order of the channel width and sediment size. Alternate bars can cause riverbanks to erode, where it is thought that bar formation can trigger incipient meandering. While alternate bars are formed due to bed instability, meandering is formed due to bank instability.

This study aims to perform linear stability analysis of the formation of sand bars on the riverbed with the use of a new bank erosion model. The process-based bank erosion model states that the time variation of bank junction is proportional to the lateral sediment transport rate at the junction between the bed and bank regions, which is evaluated by the lateral sediment transport rate in the bank region and the time variation of the bed elevation at the junction. Furthermore, the model used in the study accounts for the variability of the parameters that influence the formation of bars, and to clarify the effect of bank erosion into the analysis by determining its effect on bar wavelength.

The St. Venant shallow water equations are used as governing equations and the process-based bank erosion model is derived to its simple form following the assumptions of the study. In addition, a parameter, ϵ, is introduced in order to provide a protection that inhibits bank erosion, such as slump block armouring or the presence of vegetation. From linear stability analysis, the solutions of banks that are in-phase are obtained for the case of bar instability with and without bank erosion. The growth rates of perturbation are solved using ϵ - expansion to consider the effect of the slump block armouring or the presence of vegetation. The Chebyshev polynomials are also employed for numerical solution. If the growth rate is positive, the base state is unstable and it is considered that bars theoretically form; otherwise, the flat bed is stable and no bars grow.

The results from linear stability analysis are presented in three cases. Firstly, the parameters such as Froude number, Shields number and bed friction coefficient are varied. Secondly, the aspect ratio and the parameter that inhibits bank erosion ϵ are varied. Thirdly, the phases at the banks

and the spatial distribution of the perturbed variables are presented. In the first case, the growth rates of perturbation are plotted in the dimensionless wavenumber - aspect ratio plane, or the k-β plane. It is found that when the Froude number is increased, the unstable region shifts to a range of smaller wavenumbers or the wavelength increases. Also, when the bed friction coefficient is increased, the critical aspect ratio tends to decrease. In a similar way, when the aspect ratio is increased from $\beta = 10$ to 40, the growth rates are amplified. Meanwhile, when the Shields number is increased, the effect of bank erosion is minimized; at Shields number equal to 0.06, the effect of bank erosion is relevant.

For the second case, the growth rates are plotted against k, and β is varied from 10 to 20. The parameter that inhibits bank erosion, ϵ, is also varied from 0 to 1. As a general observation, it is found that the contours shift to a range of smaller wavenumbers and the maximum growth rates are damped when ϵ is increased. On the other hand, for $\beta = 10$ and 20, the phase diagrams and the spatial distribution diagrams reveal that the perturbation variable for the streamwise flow velocity is out-of-phase with the perturbation variable for the lateral flow velocity, while the perturbation variable for the flow depth is out-of-phase with the perturbation variable for the bed elevation. The phase diagrams also show that the perturbation progresses in the downstream direction in a periodic manner, and that left bank and the right bank perturbations are in-phase with each other, confirming that the solution is for in-phase banks.

In order to validate the theoretical results, a comparison is performed for the calculated wavelength values with wavelength values obtained from experimental studies on bar formation. The dominant wavenumber corresponding to the maximum growth rate of perturbation as obtained from stability analysis is selected as the representative wavelength for actual comparison of bar wavelength. It is found that the calculated wavelength values generally underestimate the observed wavelength values. In addition, the experimental data obtained for both erodible and non-erodible banks are plotted in the instability diagram generated for bar instability with and without bank erosion, respectively. It is revealed that the experimental data fall within the stable region. It is suggested that the aspect ratio be increased to a value higher than the critical aspect ratio obtained from the analysis.

The study concludes that the aspect ratio, Froude number, Shields number, bank slopes and roughness coefficient are the parameters that influence the formation of bars. It is found that bars are more likely to develop at low aspect ratios when the bed friction coefficient is increased. The study also reveals that the Froude number and the parameter ϵ that inhibits bank erosion influence the solution for bar instability by increasing the wavelength

of the bars, while increasing the aspect ratio and the bank slopes causes the maximum growth rates of perturbation to be amplified. Since the theoretical result can provide a rough estimate of the actual values of bar wavelength, a comparison of the theoretical and experimental results is performed. It is revealed that the observed wavelength is twice as large as the calculated wavelength values. The predicted results from the analysis generally underestimate the results of the experiment. It is possible that in the scheme of linear stability analysis, the instability process first selects the wavenumber and then enhances the growth rates of the bars; hence, bar formation in the stability analysis is slow.

Contents

List of Tables

List of Figures

Chapter 1

Introduction

Depending upon the fluid flow and sediment transport conditions, a variety of structures can develop on the riverbed whenever perturbations are induced. These include ripples, dunes, antidunes, and alternate bars. While the first three types of bedform provide a significant resistance to the flow by the river bed, control the river depth, and are periodically formed [1], alternate bars can exist together with dunes and are often formed as isolated features. These megascale bedforms arise upon the order of the channel width.

Alternate bars can cause river banks to erode; the river banks themselves contribute to the deformation of the channel planform through bank erosion. In this context, alternate bars allow for the onset of meandering. Meandering is considered to be a process of exchange of sediments from the caving banks to the depositing bars, and from the consequent local overloading and deposition of the heavier sediments as they move along the bed [2]. Fully-developed meandering requires a considerable balance between erosion and deposition from the banks [1].

Meandering in which originally straight river channels tend to become winding river channels over time has been studied as one of the most interesting processes among river evolution phenomena. Kinoshita [3] suggests that the formation of alternating sandbars triggers meandering from analysis of a great number of aerial photographs of meandering rivers. **Fig. 1.1** shows the conceptual diagram of such a process. The formation of alternating sandbars causes a water impact at the downstream edge of the sandbar (a). At the point of the water impact, bank erosion occurs (b), leading to the development of meandering (c).

Meanwhile, many theoretical studies have been done on the development of meandering and the formation of fluvial bars. If a small sinusoidal disturbance is imposed to the planar shape of river channels, the curvature of the river channel causes a deviation of the flow towards the outer bank, erosion

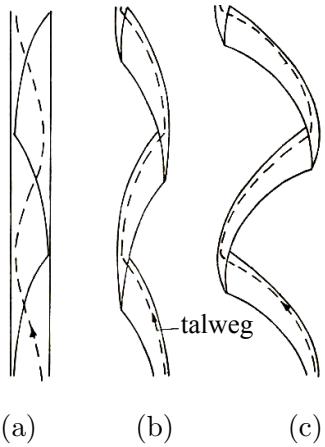

Figure 1.1: Conceptual diagram of meandering induced by fluvial bars.The formation of alternating sandbars causes a water impact at the downstream edge of the sandbar (a). At the point of the water impact, bank erosion occurs (b), leading to the development of meandering (c).

on the outer bank and accumulation on the inner bank occur, and meandering makes further development under some conditions. Theoretically, the initial development of bars can be explained in the context of linear stability analysis. In linear stability analysis, the temporal growth rate, migration speed, wavelength and spatial damping factor can be obtained. Although the values of the amplitude cannot be obtained, linear stability analysis still provides information on the temporal and spatial change of the amplitude [4]. A few studies employing linear stability analysis have also been conducted in order to obtain the characteristics of river meanders. Ikeda, Parker, Sawai [5] provided a first theoretical explanation on the mechanism of meandering as a shear instability on both banks in terms of linear stability analysis. Afterwards, the influence of interaction and resonance with fluvial bars has been taken into account from the condition satisfying the continuity of sediment [6], and the influence of secondary flow due to meandering has been included into the linear stability analysis [7]. According to these theories, the development of meandering and the formation of sand bars interact with each other. Meanwhile, in other studies, stability analysis techniques were restricted to erodible beds and fixed banks [8], such as the works of Callander [9] and Colombini et al. [10] where the latter both considered the linear and the weakly non- linear theories. Recently, however, the lateral migration of the channel has been included in order to model erodible banks. Incorporating the channel migration is important in order to better understand the

role of bank erosion in the lateral channel shift that can influence meandering. In one study, Shimada et al. [11] performed linear stability analysis on a straight channel with erodible river banks and found that bars will have longer wavelengths than the ones produced by previous bar theories. It was also found that Froude number significantly affects bar wavelength. In another study, Iwasaki et al. [12] performed both linear stability analysis and numerical simulation and focused on how the modeling of secondary flow affects free bar morphodynamics for straight open channels. Lastly, Uddin et al. [13] also employed linear stability analysis to study the stability of bars by employing the process-based bank erosion model by Parker et al. [14]. However, their results show that the perturbation is unstable everywhere in the instability diagram.

While meandering is caused by the bank instability due to the curvature of the planar geometry of a river channel, however, the formation of sand bars is caused by the bed instability between flow and the riverbed. It follows that they are basically different instability. If all meandering is to be explained by the bank instability, how should we understand the development of meandering originated from the sand bars that Kinoshita [3] observed?

In this study, we perform linear stability analysis of meandering induced by the formation of sandbars on the riverbed with the use of a new bank erosion model on the basis of the idea that meandering is not always caused by the bank instability, and that meandering is sometimes triggered by the formation of fluvial sand bars. The study also aims to determine the influence of varying the aspect ratio, Shields number, Froude number, bed friction coefficient and bank slopes to the instability of bars by evaluating their effect on bar wavelength and maximum growth rate of perturbation. Furthermore, the effect of bank erosion is clarified by varying a parameter that retards bank erosion.

Alternate bar studies can help provide relevant information on their hydraulic characteristics, such as the conditions to which they form, geometrical properties, migration velocities [15] that can aid in river restoration measures. These measures may include providing vegetation, increasing cohesion to control bank erosion, and any other means of river bank stabilization. The relevance of this study is realized by providing a representative wavelength that is thought to provide a crude estimate of bar wavelengths observed in nature, and to provide a range of aspect ratios that may predict the growth of bars for a given set of flow and sediment parameters to be utilized in an experimental set-up.

Chapter 2

Formulation

2.1 Flow and bed evolution

In this study, we perform linear stability analysis of fluvial bars in a channel with its banks subject to erosion as shown in **Fig. 2.1**. At the linear level, the lateral length scales of bars and bank erosion can be assumed to be on the same order. Flow in such a situation can be described by the shallow water equations and the continuity equation written in the form

$$\tilde{U}\frac{\partial \tilde{U}}{\partial \tilde{x}} + \tilde{V}\frac{\partial \tilde{U}}{\partial \tilde{y}} = -g\left(\frac{\partial \tilde{H}}{\partial \tilde{x}} + \frac{\partial \tilde{Z}}{\partial \tilde{x}}\right) - \frac{\tilde{T}_{bx}}{\rho \tilde{H}} \tag{2.1}$$

$$\tilde{U}\frac{\partial \tilde{V}}{\partial \tilde{x}} + \tilde{V}\frac{\partial \tilde{V}}{\partial \tilde{y}} = -g\left(\frac{\partial \tilde{H}}{\partial \tilde{y}} + \frac{\partial \tilde{Z}}{\partial \tilde{y}}\right) - \frac{\tilde{T}_{by}}{\rho \tilde{H}} \tag{2.2}$$

$$\frac{\partial \tilde{U}\tilde{H}}{\partial \tilde{x}} + \frac{\partial \tilde{V}\tilde{H}}{\partial \tilde{y}} = 0 \tag{2.3}$$

where $\tilde{x}$ and $\tilde{y}$ are the streamwise and lateral coordinates respectively, $\tilde{U}$ and $\tilde{V}$ are the $\tilde{x}$ and $\tilde{y}$ components of the velocity respectively, $\tilde{H}$ and $\tilde{Z}$ are the flow depth and the bed elevation respectively, $\tilde{T}_{bx}$ and $\tilde{T}_{by}$ are the $\tilde{x}$ and $\tilde{y}$ components of the bed shear stress respectively, ρ is the density of water ($= 1,000$ kg/m^3), and $\tilde{}$ denotes dimensional variables, and are later removed to denote non-dimensional equivalents. The $\tilde{x}$ and $\tilde{y}$ components of the bed shear stress $\tilde{T}_{bx}$ and $\tilde{T}_{by}$ are written, respectively, in the form

$$\left(\tilde{T}_{bx}, \tilde{T}_{by}\right) = \tilde{T}_b\left(\tilde{U}, \tilde{V}\right)\left(\tilde{U}^2 + \tilde{V}^2\right)^{-1/2} \tag{2.4}$$

where $\tilde{T}_b$ is the total bed shear stress, written in the form

$$\tilde{T}_b = \rho C_f\left(\tilde{U}^2 + \tilde{V}^2\right) \tag{2.5}$$

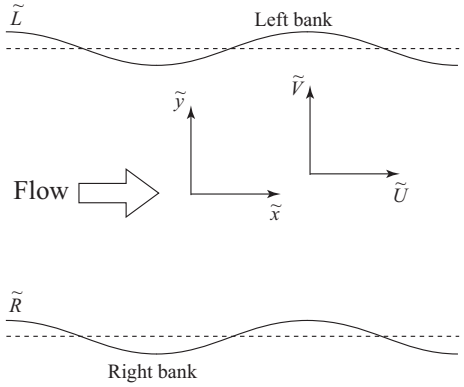

Figure 2.1: Conceptual diagram of the channel and coordinates.

where C_f is the bed friction coefficient, which is known to be a weak function of the flow depth relative to the equivalent roughness height, but is assumed to be a constant for simplicity.

The time variation of the bed elevation can be described by

$$(1-\lambda_p)\frac{\partial \tilde{Z}}{\partial \tilde{t}} + \tilde{\nabla}\cdot\tilde{\boldsymbol{Q}}_s = 0 \tag{2.6}$$

where λ_p is porosity, $\tilde{\nabla} = (\partial/\partial\tilde{x}, \partial/\partial\tilde{y})$, and $\tilde{\boldsymbol{Q}}_s$ is the sediment transport vector, and is expressed with the use of the angle between the direction of the sediment transport and the $\tilde{x}$ axis, ϕ, such that

$$\tilde{\boldsymbol{Q}}_s = \left(\tilde{Q}_{s,x}, \tilde{Q}_{s,y}\right) = \tilde{Q}_s\left(\cos\phi, \sin\phi\right) \tag{2.7}$$

where $\tilde{t}$ is time, and $\tilde{Q}_s$ is the total sediment transport rate per unit width.

Parker et al. [18] have found that Bagnold's hypothesis is not valid when the the bed has a slope in the lateral direction, and proposed a sediment transport formula applicable to the case with arbitrary bed slopes based on the balance of the forces acting on particles on the bed. The formula proposed by Parker et al. written in a vectorial form, which cannot describe the sediment transport rate in an explicit manner, is inconvenient for analytical purposes. We employ the following linearized equation assuming that the bed slope is sufficiently small:

$$\tilde{Q}_s = K\left(\theta-\theta_c\right)\left(\theta^{1/2} - 0.7\theta_c^{1/2}\right) \tag{2.8a}$$

$$\sin\phi = \frac{\tilde{V}}{\sqrt{\tilde{U}^2+\tilde{V}^2}} - \frac{r}{\theta^{1/2}}\frac{\partial \tilde{Z}}{\partial \tilde{y}} \tag{2.8b}$$

Here K is an empirical constant ($= 7.67$), and θ is the non-dimensional bed shear stress and is defined with the use of the dimensional bed shear stress by

$$\theta = \frac{\tilde{T}_b}{\rho R_s g \tilde{d}_s} \tag{2.9}$$

where R_s is the submerged specific gravity ($= 1.65$), g is the gravity acceleration ($= 9.8$ m/s^2), and $\tilde{d}_s$ is the sediment diameter. In addition, θ_c is the non-dimensional critical bed shear stress and is assumed to be a constant of 0.047, and r is an empirical constant between 0.3 and 0.5. Parker et al.'s formula reduces to the same form as the existing formula when the bed slope is sufficiently small.

2.2 Base state

The base state for linear stability analysis is the normal flow condition, in which the streamwise velocity $\tilde{U}$ and the flow depth $\tilde{H}$ are constant in time and space, the lateral velocity $\tilde{V}$ vanishes, and the bed elevation $\tilde{Z}$ does not change from the original bed elevation with a constant slope in the streamwise direction. When the streamwise bed slope is denoted by S, the bed elevation $\tilde{Z}$ can be written in the form

$$\tilde{Z}_n = \tilde{Z}_0 - S\tilde{x} \tag{2.10}$$

where the subscript n denotes variables in the normal flow condition, and $\tilde{Z}_0$ is the bed elevation when $\tilde{x} = 0$. With the use of (2.4), (2.5) and (2.10), (2.1) reduces to

$$gS - \frac{C_f \tilde{U}_n^2}{\tilde{H}_n} = 0 \tag{2.11}$$

The continuity equation (2.3) can be easily integrated to be

$$\tilde{U}_n \tilde{H}_n = \tilde{Q} \tag{2.12}$$

where $\tilde{Q}$ is the flow discharge per unit width. Solving (2.11) and (2.12), we obtain

$$\tilde{U}_n = \left(\frac{g\tilde{Q}S}{C_f}\right)^{1/3}, \quad \tilde{H}_n = \left(\frac{C_f \tilde{Q}^2}{gS}\right)^{1/3} \tag{2.13}$$

2.3 Normalization

We introduce the normalization written in the form

$$(\tilde{x}, \tilde{y}) = \tilde{B}(x, y), \quad (\tilde{U}, \tilde{V}) = \tilde{U}_n(U, V), \tag{2.14a, b}$$

$$(\tilde{H}, \tilde{Z}) = \tilde{H}_n(H, Z), \quad (\tilde{T}_{bx}, \tilde{T}_{by}) = \rho \tilde{U}_n^2 \, (T_{bx}, T_{by}) \tag{2.14c, d}$$

$$\tilde{\boldsymbol{Q}}_s = \sqrt{R_s g \tilde{d}_s}^{1/2} \boldsymbol{Q}_s, \quad \tilde{t} = \frac{(1-\lambda_p)\tilde{H}_n \tilde{B}}{\sqrt{R_s g \tilde{d}_s^3}} t \tag{2.14e, f}$$

where $\tilde{B}$ is the half width of the channel. With the use of the above normalization, the flow equations (2.1)–(2.3) are normalized to be

$$U\frac{\partial U}{\partial x} + V\frac{\partial U}{\partial y} = -F^{-2}\left(\frac{\partial H}{\partial x} + \frac{\partial Z}{\partial x}\right) - \beta \frac{T_{bx}}{H} \tag{2.15}$$

$$U\frac{\partial V}{\partial x} + V\frac{\partial V}{\partial y} = -F^{-2}\left(\frac{\partial H}{\partial y} + \frac{\partial Z}{\partial y}\right) - \beta \frac{T_{by}}{H} \tag{2.16}$$

$$\frac{\partial UH}{\partial x} + \frac{\partial VH}{\partial y} = 0 \tag{2.17}$$

where F and β are the Froude number and the aspect ratio, respectively, defined by

$$F = \frac{\tilde{U}_n}{\sqrt{g\tilde{H}_n}} \tag{2.18}$$

$$\beta = \frac{\tilde{B}}{\tilde{H}_n} \tag{2.19}$$

The non-dimensional bed shear stress vector is

$$(T_{bx}, T_{by}) = T_b \, (U, V) \left(U^2 + V^2\right)^{-1/2} \tag{2.20}$$

$$T_b = C_f \left(U^2 + V^2\right) \tag{2.21}$$

The equation describing the time variation of the bed elevation can be normalized in the form

$$\frac{\partial Z}{\partial t} + \nabla \cdot \boldsymbol{Q}_s = 0 \tag{2.22}$$

where $\nabla = (\partial/\partial x, \partial/\partial y)$, and

$$\boldsymbol{Q}_s = (Q_{s,x}, Q_{s,y}) = Q_s \, (\cos\phi, \sin\phi) \tag{2.23}$$

$$Q_s = K \, (\theta - \theta_c) \left(\theta^{1/2} - 0.7\theta_c^{1/2}\right) \tag{2.24a}$$

$$\sin\phi = \frac{V}{\sqrt{U^2 + V^2}} - \frac{r}{\beta\theta^{1/2}} \frac{\partial Z}{\partial y} \tag{2.24b}$$

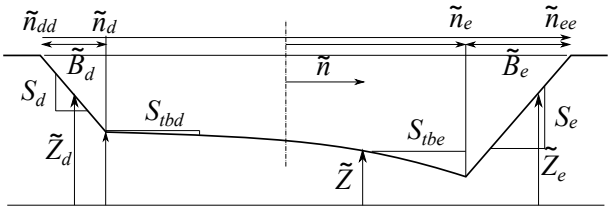

Figure 2.2: Conceptual model of bank erosion.

2.4 Bank erosion model

Modifying and improving the bank erosion models proposed by Ikeda [5] and Hasegawa [17], Parker et al. [14] have proposed the following model.

With the use of the coordinates attached to the center line of a channel, the sediment continuity equation can be written in the form

$$(1-\lambda_p)\left(1+\tilde{C}\tilde{n}\right)\frac{\partial \tilde{Z}}{\partial \tilde{t}} = -\frac{\partial \tilde{Q}_{s,s}}{\partial \tilde{s}} - \frac{\partial}{\partial \tilde{n}}\left[\left(1+\tilde{C}\tilde{n}\right)\tilde{Q}_{s,n}\right] \tag{2.25}$$

where $\tilde{s}$ and $\tilde{n}$ are the coordinates tangential and normal to the center line of the channel respectively, $\tilde{Q}_{s,s}$ and $\tilde{Q}_{s,n}$ are the $\tilde{s}$ and $\tilde{n}$ components of the sediment transport rate respectively, and $\tilde{C}$ is the curvature of the center line. The above equation holds in the bed region, and the equation in the eroding bank and depositing bank regions can be written with the subscripts e and d respectively in the form

$$(1-\lambda_p)\left(1+\tilde{C}\tilde{n}\right)\frac{\partial \tilde{Z}_e}{\partial \tilde{t}} = -\frac{\partial \tilde{Q}_{se,s}}{\partial \tilde{s}} - \frac{\partial}{\partial \tilde{n}}\left[\left(1+\tilde{C}\tilde{n}\right)\tilde{Q}_{se,n}\right] \tag{2.26}$$

$$(1-\lambda_p)\left(1+\tilde{C}\tilde{n}\right)\frac{\partial \tilde{Z}_d}{\partial \tilde{t}} = -\frac{\partial \tilde{Q}_{sd,s}}{\partial \tilde{s}} - \frac{\partial}{\partial \tilde{n}}\left[\left(1+\tilde{C}\tilde{n}\right)\tilde{Q}_{sd,n}\right] \tag{2.27}$$

Integrating (2.26) over the whole eroding bank region, we obtain the equation of the form

$$(1-\lambda_p)\int_{\tilde{n}_e}^{\tilde{n}_{ee}}\left(1+\tilde{C}\tilde{n}\right)\frac{\partial \tilde{Z}_e}{\partial \tilde{t}}\mathrm{d}\tilde{n} = -\int_{\tilde{n}_e}^{\tilde{n}_{ee}}\frac{\partial \tilde{Q}_{se,s}}{\partial \tilde{s}}\mathrm{d}\tilde{n} - \int_{\tilde{n}_e}^{\tilde{n}_{ee}}\frac{\partial}{\partial \tilde{n}}\left[\left(1+\tilde{C}\tilde{n}\right)\tilde{Q}_{se,n}\right]\mathrm{d}\tilde{n} \tag{2.28}$$

where $\tilde{n}_e$ is the $\tilde{n}$ coordinate at the junction between the bed and eroding bank regions, and $\tilde{n}_{ee}$ is the $\tilde{n}$ coordinate of the outer bound of the eroding bank region. Note that both $\tilde{n}_e$ and $\tilde{n}_{ee}$ are functions of time, and therefore, the eroding bank region always ranges between $\tilde{n} = \tilde{n}_e$ and $\tilde{n}_{ee}$. Assuming

the lateral bed slope in the eroding bank region is a constant S_e, the bed elevation $\tilde{Z}_e$ can be written in the form

$$\tilde{Z}_e\left(\tilde{s},\tilde{n},\tilde{t}\right)=\tilde{Z}\left(\tilde{s},\tilde{n}_e(t),\tilde{t}\right)+S_e\left(\tilde{n}-\tilde{n}_e\right) \tag{2.29}$$

Taking the time derivative of the above equation, we obtain

$$\begin{aligned}\frac{\partial\tilde{Z}_e}{\partial\tilde{t}} &= \left.\frac{\partial\tilde{Z}}{\partial\tilde{t}}\right|_{\tilde{n}=\tilde{n}_e}+\left.\frac{\partial\tilde{Z}}{\partial\tilde{n}}\right|_{\tilde{n}=\tilde{n}_e}\frac{\partial\tilde{n}_e}{\partial\tilde{t}}-S_e\frac{\partial\tilde{n}_e}{\partial\tilde{t}}\\ &= \left.\frac{\partial\tilde{Z}}{\partial\tilde{t}}\right|_{\tilde{n}=\tilde{n}_e}+\left.\frac{\partial\tilde{Z}}{\partial\tilde{n}}\right|_{\tilde{n}=\tilde{n}_e}\dot{\tilde{n}}_e-S_e\dot{\tilde{n}}_e\\ &= \left.\frac{\partial\tilde{Z}}{\partial\tilde{t}}\right|_{\tilde{n}=\tilde{n}_e}-\left(S_e+S_{tbe}\right)\dot{\tilde{n}}_e\end{aligned} \tag{2.30}$$

where

$$S_{tbe}=-\left.\frac{\partial\tilde{Z}}{\partial\tilde{n}}\right|_{\tilde{n}=\tilde{n}_e} \tag{2.31}$$

The physical implication of the above equation is illustrated in **Fig. 2.3**. As shown in this figure, the relation between the time variation of the location of the eroding bank $\dot{\tilde{n}}_e$ and the time variation of the bed elevation where $\tilde{n}=\tilde{n}_e$ is

$$\begin{aligned}-\frac{\partial\tilde{Z}_e}{\partial\tilde{t}}\Delta\tilde{t} &= \left(S_e\dot{\tilde{n}}_e\Delta\tilde{t}-\left.\frac{\partial\tilde{Z}}{\partial\tilde{t}}\right|_{\tilde{n}=\tilde{n}_e}\Delta\tilde{t}\right)+S_{tbe}\dot{\tilde{n}}_e\Delta\tilde{t}\\ &= -\left.\frac{\partial\tilde{Z}}{\partial\tilde{t}}\right|_{\tilde{n}=\tilde{n}_e}\Delta\tilde{t}+\left(S_e+S_{tbe}\right)\dot{\tilde{n}}_e\Delta\tilde{t}\end{aligned} \tag{2.32}$$

This is equivalent to (2.30).

Substituting (2.30), we obtain the left hand side of (2.28) in the form

$$\left(1-\lambda_p\right)\int_{\tilde{n}_e}^{\tilde{n}_{ee}}\left(1+\tilde{C}\tilde{n}\right)\frac{\partial\tilde{Z}_e}{\partial\tilde{t}}\mathrm{d}\tilde{n}=\left(1-\lambda_p\right)\tilde{B}_e\left(1+\tilde{C}\bar{\tilde{n}}_e\right)\left[\left.\frac{\partial\tilde{Z}}{\partial\tilde{t}}\right|_{\tilde{n}=\tilde{n}_e}-\left(S_e+S_{tbe}\right)\dot{\tilde{n}}_e\right] \tag{2.33}$$

The first term of the right hand side of (2.28) becomes

$$-\int_{\tilde{n}_e}^{\tilde{n}_{ee}}\frac{\partial\tilde{Q}_{se,s}}{\partial\tilde{s}}\mathrm{d}\tilde{n}=-\frac{\partial}{\partial\tilde{s}}\int_{\tilde{n}=\tilde{n}_e}^{\tilde{n}=\tilde{n}_{ee}}\tilde{Q}_{se,s}\mathrm{d}\tilde{n}+\frac{\partial\tilde{n}_{ee}}{\partial\tilde{s}}\left.\tilde{Q}_{se,s}\right|_{\tilde{n}=\tilde{n}_{ee}}-\frac{\partial\tilde{n}_e}{\partial\tilde{s}}\left.\tilde{Q}_{se,s}\right|_{\tilde{n}=\tilde{n}_e} \tag{2.34}$$

The sediment transport in the streamwise direction at the outer bound of the eroding bank region $\tilde{Q}_{se,s}|_{\tilde{n}=\tilde{n}_{ee}}$ should vanish, and therefore, the above

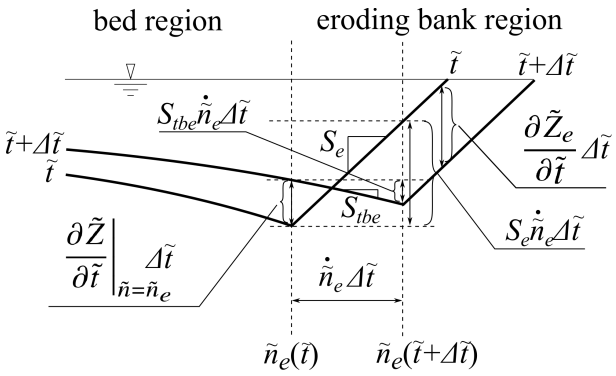

Figure 2.3: Physical implication of (2.30).

equation reduces to

$$-\int_{\tilde{n}_e}^{\tilde{n}_{ee}} \frac{\partial \tilde{Q}_{se,s}}{\partial \tilde{s}} \mathrm{d}\tilde{n} = -\frac{\partial}{\partial \tilde{s}} \int_{\tilde{n}=\tilde{n}_e}^{\tilde{n}=\tilde{n}_{ee}} \tilde{Q}_{se,s} \mathrm{d}\tilde{n} - \frac{\partial \tilde{n}_e}{\partial \tilde{s}} \left. \tilde{Q}_{se,s} \right|_{\tilde{n}=\tilde{n}_e} \tag{2.35}$$

The second term of the right hand side of (2.29) becomes

$$-\int_{\tilde{n}_e}^{\tilde{n}_{ee}} \frac{\partial}{\partial \tilde{n}} \left[\left(1+\tilde{C}\tilde{n}\right) \tilde{Q}_{se,n} \right] \mathrm{d}\tilde{n} = -\left(1+\tilde{C}\tilde{n}_{ee}\right) \left. \tilde{Q}_{se,n} \right|_{\tilde{n}=\tilde{n}_{ee}} + \left(1+\tilde{C}\tilde{n}_e\right) \left. \tilde{Q}_{se,n} \right|_{\tilde{n}=\tilde{n}_e} \tag{2.36}$$

The sediment transport through the outer bound of the eroding bank region $\tilde{Q}_{se,n}|_{\tilde{n}=\tilde{n}_{ee}}$ should vanish, and therefore, the above equation reduces to

$$-\int_{\tilde{n}_e}^{\tilde{n}_{ee}} \frac{\partial}{\partial \tilde{n}} \left[\left(1+\tilde{C}\tilde{n}\right) \tilde{Q}_{se,n} \right] \mathrm{d}\tilde{n} = \left(1+\tilde{C}\tilde{n}_e\right) \left. \tilde{Q}_{se,n} \right|_{\tilde{n}=\tilde{n}_e} \tag{2.37}$$

Combining (2.33), (2.35) and (2.37), we obtain the following equation:

$$\begin{aligned} (1-\lambda_p)\,\tilde{B}_e \left(1+\tilde{C}\tilde{\bar{n}}_e\right) \left[\left. \frac{\partial \tilde{Z}}{\partial \tilde{t}} \right|_{\tilde{n}=\tilde{n}_e} - \left(S_e + S_{tbe}\right) \dot{\tilde{n}}_e \right] \;=\; & -\frac{\partial}{\partial \tilde{s}} \int_{\tilde{n}=\tilde{n}_e}^{\tilde{n}=\tilde{n}_{ee}} \tilde{Q}_{se,s} \mathrm{d}\tilde{n} - \frac{\partial \tilde{n}_e}{\partial \tilde{s}} \left. \tilde{Q}_{se,s} \right|_{\tilde{n}=\tilde{n}_e} \\ & + \left(1+\tilde{C}\tilde{n}_e\right) \left. \tilde{Q}_{se,n} \right|_{\tilde{n}=\tilde{n}_e} \end{aligned} \tag{2.38}$$

Solving the above equation for $\dot{\tilde{n}}_e$, we obtain

$$\frac{\partial \tilde{n}_e}{\partial \tilde{t}} = \frac{1}{S_e + S_{tbe}} \left[\frac{\frac{\partial}{\partial \tilde{s}} \int_{\tilde{n}_e}^{\tilde{n}_{ee}} \tilde{Q}_{se,s} \mathrm{d}\tilde{n} + \left(1+\tilde{C}\tilde{n}_e\right) \tilde{Q}_{fe,j}}{(1-\lambda_p)\tilde{B}_e(1+\tilde{C}\tilde{\bar{n}}_e)} + \left. \frac{\partial \tilde{Z}}{\partial \tilde{t}} \right|_{\tilde{n}=\tilde{n}_e} \right] \tag{2.39}$$

where $Q_{fe,j}$ is the sediment transport rate in the direction normal to the bank line $n = n_e$ from the eroding bank to bed regions, written in the form

$$\left(1+\tilde{C}\tilde{n}_e\right) \tilde{Q}_{fe,j} = \frac{\partial \tilde{n}_e}{\partial \tilde{s}} \left. \tilde{Q}_{se,s} \right|_{\tilde{n}=\tilde{n}_e} - \left(1+\tilde{C}\tilde{n}_e\right) \left. \tilde{Q}_{se,n} \right|_{\tilde{n}=\tilde{n}_e} \tag{2.40}$$

The bed elevation in the depositing bank region $\tilde{Z}_d$ is

$$\tilde{Z}_d = \tilde{Z}(\tilde{s}, \tilde{n}_d(\tilde{t}), \tilde{t}) - S_d(\tilde{n} - \tilde{n}_d) \tag{2.41}$$

Therefore, the time variation of the bed elevation in the depositing bank region is

$$\begin{aligned} \frac{\partial \tilde{Z}_d}{\partial \tilde{t}} &= \left.\frac{\partial \tilde{Z}}{\partial \tilde{t}}\right|_{\tilde{n}=\tilde{n}_d} + \left.\frac{\partial \tilde{Z}}{\partial \tilde{n}}\right|_{\tilde{n}=\tilde{n}_d} \dot{\tilde{n}}_d + S_d \dot{\tilde{n}}_d \\ &= \left.\frac{\partial \tilde{Z}}{\partial \tilde{t}}\right|_{\tilde{n}=\tilde{n}_d} + (S_d - S_{tbd})\, \dot{\tilde{n}}_d \end{aligned} \tag{2.42}$$

where S_d is the lateral slope in the depositing bank region, and S_{tbd} is the lateral bed slope where $\tilde{n} = \tilde{n}_d$ in the bed region, defined by

$$S_{tbd} = -\left.\frac{\partial \tilde{Z}}{\partial \tilde{n}}\right|_{\tilde{n}=\tilde{n}_d} \tag{2.43}$$

Integrating (2.27) from $\tilde{n}_{ee}$ to $\tilde{n}_e$, we obtain

$$\begin{aligned} (1-\lambda_p) \int_{\tilde{n}_{dd}}^{\tilde{n}_d} \left(1 + \tilde{C}\tilde{n}\right) \mathrm{d}\tilde{n} \quad & \left[\left.\frac{\partial \tilde{Z}}{\partial \tilde{t}}\right|_{\tilde{n}=\tilde{n}_d} + (S_d - S_{tbd})\, \dot{\tilde{n}}_d \right] \\ &= -\int_{\tilde{n}_{dd}}^{\tilde{n}_d} \frac{\partial \tilde{Q}_{sd,s}}{\partial \tilde{s}} \mathrm{d}\tilde{n} - \int_{\tilde{n}_{dd}}^{\tilde{n}_d} \frac{\partial}{\partial \tilde{n}} \left[\left(1 + \tilde{C}\tilde{n}\right) \tilde{Q}_{sd,n} \right] \mathrm{d}\tilde{n} \\ &= -\frac{\partial}{\partial \tilde{s}} \int_{\tilde{n}_{dd}}^{\tilde{n}_d} Q_{sd,s} \mathrm{d}\tilde{n} + \left(1 + \tilde{C}\tilde{n}_d\right) \tilde{Q}_{fd,j} \end{aligned} \tag{2.44}$$

where $\tilde{Q}_{fd,j}$ is the sediment transport rate in the direction normal to the line of the depositing bank from the bed to depositing bank regions, written in the form

$$\left(1 + \tilde{C}\tilde{n}_d\right) \tilde{Q}_{fd,j} = \frac{\partial \tilde{n}_d}{\partial \tilde{s}}\, \tilde{Q}_{sd,s}\Big|_{\tilde{n}=\tilde{n}_d} - \left(1 + \tilde{C}\tilde{n}_d\right) \tilde{Q}_{sd,n}\Big|_{\tilde{n}=\tilde{n}_d} \tag{2.45}$$

Solving (2.44) for $\dot{\tilde{n}}_d$, we obtain

$$\frac{\partial \tilde{n}_d}{\partial \tilde{t}} = -\frac{1}{S_d - S_{tbd}} \left[\left.\frac{\partial \tilde{Z}}{\partial \tilde{t}}\right|_{\tilde{n}=\tilde{n}_d} + \frac{\frac{\partial}{\partial \tilde{s}} \int_{\tilde{n}_{dd}}^{\tilde{n}_d} \tilde{Q}_{sd,s}\, \mathrm{d}\tilde{n} - (1 + \tilde{C}\tilde{n}_d) \tilde{Q}_{fd,j}}{(1-\lambda_p) \tilde{B}_d (1 + \tilde{C}\tilde{\tilde{n}}_d)} \right] \tag{2.46}$$

where $\tilde{\tilde{n}}_d$ is $(\tilde{n}_d + \tilde{n}_{dd})/2$, and $\tilde{B}_d$ is the width of the depositing bank region.

In (2.39) and (2.46), while the sediment transport in the $\tilde{n}$ direction causes bank erosion directly, the $\tilde{s}$ derivative of the sediment transport in the

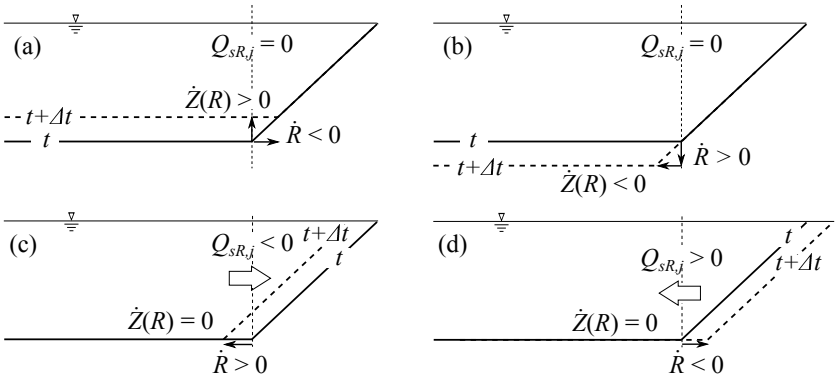

Figure 2.4: Right bank evolutions. (a) Apparent bank erosion due to bed aggradation, (b) apparent bank deposition due to bed degradation, (c) bank deposition due to sediment transport, and (d) bank erosion due to sediment transport.

$\tilde{s}$ direction causes bank erosion. In the linear stability analysis performed in this study, the variation of the sediment transport rate in the $\tilde{s}$ direction is expected not to be so large, and therefore, it should not make a significant contribution to bank erosion. Thus, we ignore the terms $\partial\left(\int_{\tilde{n}_e}^{\tilde{n}_{ee}} \tilde{Q}_{se,s}\mathrm{d}\tilde{n}\right)/\partial\tilde{s}$ and $\partial\left(\int_{\tilde{n}_d}^{\tilde{n}_{dd}} \tilde{Q}_{sd,s}\mathrm{d}\tilde{n}\right)/\partial\tilde{s}$ in (2.39) and (2.46). In addition, the bed slope in the $\tilde{n}$ direction in the eroding and depositing bank regions S_e and S_d respectively are much larger than the bed slope in the $\tilde{n}$ direction at the junction points in the bed region S_{tbe} and S_{tbd}. Ignoring S_{tbe} and S_{tbd}, and normalizing (2.39) and (2.46), we obtain the following equations:

$$\frac{\partial n_e}{\partial t} = \frac{1}{\beta S_e}\left[\frac{(1+Cn_e)Q_{fe,j}}{B_e(1+C\bar{n}_e)} + \frac{\partial Z}{\partial t}\bigg|_{n=n_e}\right] = \frac{1+Cn_e}{1+C\bar{n}_e}Q_{fe,j} + \frac{1}{\beta S_e}\frac{\partial Z}{\partial t}\bigg|_{n=n_e} \tag{2.47}$$

$$\frac{\partial n_d}{\partial t} = \frac{1}{\beta S_d}\left[\frac{(1+Cn_d)Q_{fd,j}}{B_d(1+C\bar{n}_d)} - \frac{\partial Z}{\partial t}\bigg|_{n=n_d}\right] = \frac{1+Cn_d}{1+C\bar{n}_d}Q_{fd,j} - \frac{1}{\beta S_d}\frac{\partial Z}{\partial t}\bigg|_{n=n_d} \tag{2.48}$$

where we assume $\beta = \tilde{B}/\tilde{H}_n$, $S_e = \tilde{H}_n/\tilde{B}_e$, $S_d = \tilde{H}_n/\tilde{B}_d$ and $B_e = \tilde{B}_e/\tilde{B}$, and therefore, $\beta S_e B_e = \tilde{B}/\tilde{H}_n \cdot \tilde{H}_n/\tilde{B}_e \cdot \tilde{B}_e/\tilde{B} = 1$, and $\beta S_d B_d = \tilde{B}/\tilde{H}_n \cdot \tilde{H}_n/\tilde{B}_d \cdot \tilde{B}_d/\tilde{B} = 1$. These relations have been used to simplify the above equations.

We apply the above equations to the right and left banks. Note that the $\tilde{y}$ axis is directed from right to left as shown in **Fig. 2.2**, which is opposite to the $\tilde{n}$ axis cosidered in this section. The time variation of the right bank

location R is described in the form

$$\frac{\partial R}{\partial t} = -\frac{1+CR}{1+C\bar{R}}Q_{sR,j} - \frac{1}{\beta S_R}\frac{\partial Z}{\partial t}\Big|_{y=R} \tag{2.49}$$

where S_R is the lateral slope of the right bank, $Q_{sR,j}$ is the sediment transport rate from the right bank to bed regions, B_R is the width of the right bank, and $\bar{R}$ is $R + B_R/2$.

Let us see the physical implication of the above equation by considering a simple example in detail. The conceptual diagram of right bank evolutions is shown in **Fig. 2.4**, in which the channel cross-section around the right bank at some time t is drawn by the solid line while that at $t + \Delta t$ is drawn by the dashed line. In order to clarify the role of bed elevation changes at the junction point between the right bank and bed regions, we assume that the sediment transport vanishes ($Q_{sR,j} = 0$) as illustrated in **Fig. 2.4**(a) and (b). When the bed elevation at the junction point increases ($\dot{Z}(R) > 0$), it appears that the position of the right bank moves to the right (negative direction, $\dot{R} < 0$). When the bed elevation at the junction point decreases ($\dot{Z}(R) < 0$) however, it appears that the position of the right bank moves to the left (positive direction, $\dot{R} > 0$). As such, R increases with decreasing $Z(R)$ while R decreases with increasing $Z(R)$. This can be properly described by (2.49).

The role of the lateral sediment transport can be clarified in **Fig. 2.4**(c) and (d), in which the bed elevation at the right bank line is assumed not to change ($\dot{Z}(R) = 0$). As illustrated in **Fig. 2.4**(c), the right bank advances ($\dot{R} > 0$) when $Q_{sR,j}$ is directed from the left to the right ($Q_{sR,j} < 0$). Meanwhile, the right bank retreats ($\dot{R} < 0$) when $Q_{sR,j}$ is directed from the right to the left ($Q_{sR,j} > 0$) as shown in (d). Positive and negative $Q_{sR,j}$ correspond to negative and positive $\dot{R}$. This can be also described by (2.49).

The time evolution of the location of the left bank L is described in the form

$$\frac{\partial L}{\partial t} = -\frac{1+CL}{1+C\bar{L}}Q_{sL,j} + \frac{1}{\beta S_L}\frac{\partial Z}{\partial t}\Big|_{y=L} \tag{2.50}$$

where S_L is the lateral slope in the left bank region, $Q_{sL,j}$ is the sediment transport rate from the bed to left bank regions, B_L is the width of the left bank, and $\bar{L}$ is $L + B_L/2$. The roles of the bed elevation change at the junction point and the sediment transport through the junction point are demonstrated in **Fig. 2.5**. In (a) and (b), the sediment transport rate is assumed to vanish. Then, the bed aggradation ($\dot{Z}(L) > 0$) results in the apparent bank retreat ($\dot{L} > 0$) as shown in **Fig. 2.5**(a), and the bed degradation ($\dot{Z}(L) < 0$) results in the apparent bank advance ($\dot{L} < 0$) as shown in **Fig. 2.5**(b). In (c) and (d), the bed elevation at the junction

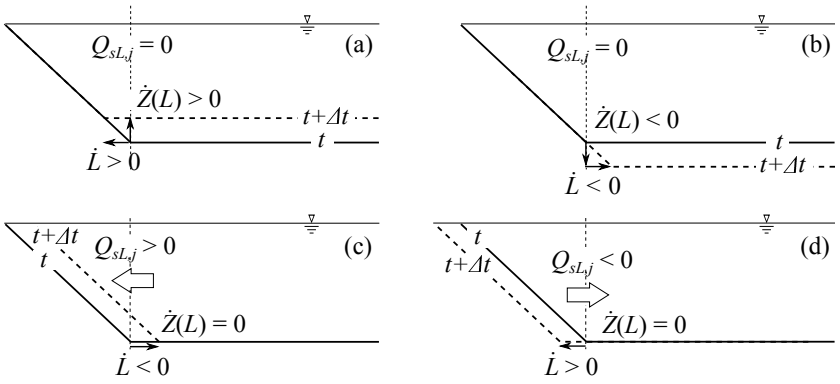

Figure 2.5: Left bank evolutions. (a) Apparent bank erosion due to bed aggradation, (b) apparent bank deposition due to bed degradation, (c) bank deposition due to sediment transport, and (d) bank erosion due to sediment transport.

point is assumed not to change. In that case, the left bank retreats ($\dot{L} > 0$) when the sediment transport is directed from the left bank to bed regions ($Q_{sL,j} < 0$) while the left bank advances ($\dot{L} < 0$) when the sediment transport is directed from the right to the left ($Q_{sL,j} > 0$). These processes can be properly described by (2.50) as well.

The sediment transport rate from the right bank to bed regions $Q_{sR,j}$, and from the bed to left bank regions $Q_{sL,j}$, are assumed to be described by an equation of the form similar to (2.23) and (2.24). In order to apply to the bank regions, we modify (2.23) and (2.24) into the form

$$Q_{sR,j} = \epsilon K(\theta - \theta_n)\left(\theta^{1/2} - 0.7\theta_n^{1/2}\right)\left(\frac{V}{U^2+V^2} + \frac{r}{\beta\theta^{1/2}}S_R\right)\Big|_{y=R} \tag{2.51}$$

$$Q_{sL,j} = \epsilon K(\theta - \theta_n)\left(\theta^{1/2} - 0.7\theta_n^{1/2}\right)\left(\frac{V}{U^2+V^2} - \frac{r}{\beta\theta^{1/2}}S_L\right)\Big|_{y=L} \tag{2.52}$$

where the non-dimensional bed shear stress in the base state normal flow condition θ_n is used in place of the non-dimensional critical bed shear stress θ_c. We employ a crude assumption that the channel is in a critical state so that the sediment transport takes place in the bank regions if the bed shear stress is even slightly larger than that in the base state.

In addition, the sediment transport does not cease even if the bed shear stress is less than the critical shear stress, and changes direction of the sediment transport. Let us ignore the lateral velocity V because it vanishes in the bank region as described later. When $\theta > \theta_n$, $Q_{sR,j}$ and $Q_{sL,j}$ are positive and negative, respectively, resulting in bank erosion in the both cases.

When $0.49\theta_n < \theta < \theta_n$ however, $Q_{sR,j}$ and $Q_{sL,j}$ are negative and positive, respectively, resulting in bank deposition in the both cases. Though (2.51) and (2.52) cannot describe the bank deposition, we extend the scope of these equations and apply them to the case of deposition.

Furthermore, ϵ is a parameter describing the effect of some protection for erosion such as slump block and vegetation. Parker et al. [14] concluded that, if bank erosion on a bank proceeds too fast, deposition on the other bank cannot catch up with the erosion. Then, the channel widening does not stop, and a constant width cannot be maintained. In order to keep a constant channel width, bank erosion should be sufficiently slowed down by some protection such as slump blocks and vegetation. Parker et al. employ a coefficient taking a value between 0 and 1 to introduce the effect of slump blocks composed of fine cohesive material covering the surface of flood plains. The coefficient ϵ is also assumed to take a relatively small value herein.

2.5 Boundary conditions

Assuming that the locations of the banks are functions of time, we denote the y coordinates of the right and left banks by R and L, respectively. Flow cannot penetrate the both banks, so that normal component of the flow must vanish. That is, we have the relations of the form

$$\boldsymbol{U} \cdot \boldsymbol{e}_{NR} = 0 \quad \text{at} \quad y = R \tag{2.53}$$

$$\boldsymbol{U} \cdot \boldsymbol{e}_{NL} = 0 \quad \text{at} \quad y = L \tag{2.54}$$

Note that the quasi-steady approximation has been used as in the case of the shallow water equations. In the above equation, $\boldsymbol{U}$ is the velocity vector $(= (U, V))$. In addition, $\boldsymbol{e}_{NL}$ and $\boldsymbol{e}_{NR}$ are the unit vector normal to the left and right banks respectively, written in the form

$$\boldsymbol{e}_{NL} = \frac{(-\partial L/\partial x, 1)}{\sqrt{1 + (\partial L/\partial x)^2}}, \quad \boldsymbol{e}_{NR} = \frac{(-\partial R/\partial x, 1)}{\sqrt{1 + (\partial R/\partial x)^2}} \tag{2.55a, b}$$

While, when the banks are immobile, the sediment transport rate through the banks should vanish, when the banks move due to erosion and deposition, it does not vanish. The boundary conditions at the right and left banks, respectively, read

$$\boldsymbol{Q}_s(R) \cdot \boldsymbol{e}_{NR} = Q_{sR,j} \tag{2.56}$$

$$\boldsymbol{Q}_s(L) \cdot \boldsymbol{e}_{NL} = Q_{sL,j} \tag{2.57}$$

Chapter 3

Linear stability analysis

3.1 Asymptotic expansions

All the variables are expanded into the base state and the perturbation imposed on the base state. Assuming that the perturbation is a sinusoidal form, which has the amplitude A, the wavelength k, and the complex angular frequency ω, we introduce the following asymptotic expansions:

$$(U, V, H, Z, R, L) = (1, 0, 1, -\beta S x, -1, 1) + A\,(U_1, V_1, H_1, Z_1, R_1, L_1)\,\mathrm{e}^{\mathrm{i}(kx-\omega t)} + \text{c.c.} \tag{3.1}$$

Here c.c. denotes the complex conjugate of the preceding terms, and $\tilde{Z}_0/\tilde{H}_n$ is assumed to vanish without losing generality. In the linear stability analysis, the very beginning of the growth process of small perturbation is studied, and therefore, the amplitude of the perturbation A is assumed to be infinitesimally small. Substituting the above equations into (2.15)–(2.17), and (2.22), and linearizing with respect to the small parameter A, we obtain equations on each order of A. At $O(A)$, we obtain

$$a_1 U_1 + a_2 H_1 + a_3 Z_1 = 0 \tag{3.2}$$

$$a_4 V_1 + a_5 \frac{\mathrm{d}H_1}{\mathrm{d}y} + a_5 \frac{\mathrm{d}Z_1}{\mathrm{d}y} = 0 \tag{3.3}$$

$$a_6 U_1 + \frac{\mathrm{d}V_1}{\mathrm{d}y} + a_6 H_1 = 0 \tag{3.4}$$

$$-\mathrm{i}\omega Z_1 + a_7 U_1 + a_8 \frac{\mathrm{d}V_1}{\mathrm{d}y} + a_9 \frac{\mathrm{d}^2 Z_1}{\mathrm{d}y^2} = 0 \tag{3.5}$$

where

$$a_1 = \mathrm{i}k + 2\beta C_f, \quad a_2 = \mathrm{i}kF^{-2} - \beta C_f, \quad a_3 = \mathrm{i}kF^{-2}, \quad a_4 = \mathrm{i}k + \beta C_f \tag{3.6a–d}$$

$$a_5 = F^{-2}, \quad a_6 = \mathrm{i}k, \quad a_7 = \mathrm{i}kK\theta_n^{1/2}\left[3\theta_n - \theta_c^{1/2}\left(1.4\theta_n^{1/2} + \theta_c^{1/2}\right)\right] \quad (3.6e\text{–}g)$$

$$a_8 = K\left(\theta_n - \theta_c\right)\left(\theta_n^{1/2} - 0.7\theta_c^{1/2}\right), \quad a_9 = -K\left(\theta_n - \theta_c\right)\left(\theta_n^{1/2} - 0.7\theta_c^{1/2}\right)\frac{r}{\beta\theta_n^{1/2}} \quad (3.6h, i)$$

where θ_n is the Shields number defined by

$$\theta_n = \frac{C_f \tilde{U}_n^2}{R_s g \tilde{d}_s} \tag{3.7}$$

The boundary conditions (2.53) and (2.54) reduce to

$$\boldsymbol{U}\cdot\boldsymbol{e}_{NR}|_{y=R} = -U(R)\frac{\partial R}{\partial x} + V(R) = A\left[-\mathrm{i}kR_1 + V_1(-1)\right]\exp\left[\mathrm{i}(kx-\omega t)\right] + \text{c.c.} = 0 \tag{3.8}$$

$$\boldsymbol{U}\cdot\boldsymbol{e}_{NL}|_{y=L} = -U(L)\frac{\partial L}{\partial x} + V(L) = A\left[-\mathrm{i}kL_1 + V_1(1)\right]\exp\left[\mathrm{i}(kx-\omega t)\right] + \text{c.c.} = 0 \tag{3.9}$$

From the above equations, we obtain the following boundary conditions at $O(A)$:

$$\mathrm{i}kR_1 - V_1(-1) + \text{c.c.} = 0 \tag{3.10}$$

$$\mathrm{i}kL_1 - V_1(1) + \text{c.c.} = 0 \tag{3.11}$$

The boundary conditions for the continuity of the sediment transport rate at the junction between the bank and bed regions can be reduced to the following. The left hand sides of (2.56) and (2.57) are, respectively

$$\begin{aligned}\boldsymbol{Q}_s\cdot\boldsymbol{e}_{NR}|_{y=R} &= -Q_{s,x}(R)\frac{\partial R}{\partial x} + Q_{s,y}(R)\\ &= AQ_{s0}\left(-\mathrm{i}kR_1 + V_1(-1) - \frac{r}{\beta\theta_n^{1/2}}\left.\frac{\mathrm{d}Z_1}{\mathrm{d}y}\right|_{y=-1}\right)\mathrm{e}^{\mathrm{i}(kx-\omega t)} + \text{c.c.}\end{aligned} \tag{3.12}$$

$$\begin{aligned}\boldsymbol{Q}_s\cdot\boldsymbol{e}_{NL}|_{y=L} &= -Q_{s,x}(L)\frac{\partial L}{\partial x} + Q_{s,y}(L)\\ &= AQ_{s0}\left(-\mathrm{i}kL_1 + V_1(1) - \frac{r}{\beta\theta_n^{1/2}}\left.\frac{\mathrm{d}Z_1}{\mathrm{d}y}\right|_{y=1}\right)\mathrm{e}^{\mathrm{i}(kx-\omega t)} + \text{c.c.}\end{aligned} \tag{3.13}$$

where $Q_{s0} = K(\theta_n - \theta_c)(\theta_n^{1/2} - 0.7\theta_c^{1/2})$. Meanwhile, the sediment transport rates in the right and left bank regions adjacent to the junction points $Q_{sR,j}$ and $Q_{sL,j}$ are, respectively, expanded into

$$Q_{sR,j} = A\epsilon\frac{0.6K\theta_n r S_R}{\beta}U_1(-1)\mathrm{e}^{\mathrm{i}(kx-\omega t)} + \text{c.c.} \tag{3.14}$$

$$Q_{sL,j} = -A\epsilon \frac{0.6K\theta_n r S_L}{\beta} U_1(1) \mathrm{e}^{\mathrm{i}(kx-\omega t)} + \text{c.c.} \tag{3.15}$$

Note that the lateral sediment transport in the right and left bank regions have positive and negative quantities, respectively, as long as U_1 is positive, as seen in the above equations. The sediment transport rate at the junction points should be continous, such that

$$Q_{s0}\left[-\mathrm{i}kR_1 + V_1(-1) - \frac{r}{\beta\theta_n^{1/2}} \frac{\mathrm{d}Z_1}{\mathrm{d}y}\bigg|_{y=-1}\right] - \epsilon \frac{0.6K\theta_n r S_R}{\beta} U_1(-1) + \text{c.c.} = 0 \tag{3.16a}$$

$$Q_{s0}\left[-\mathrm{i}kL_1 + V_1(1) - \frac{r}{\beta\theta_n^{1/2}} \frac{\mathrm{d}Z_1}{\mathrm{d}y}\bigg|_{y=1}\right] + \epsilon \frac{0.6K\theta_n r S_L}{\beta} U_1(1) + \text{c.c.} = 0 \tag{3.16b}$$

With the use of (3.10) and (3.11), the above two relations reduce to

$$-\frac{Q_{s0} r}{\beta\theta_n^{1/2}} \frac{\mathrm{d}Z_1}{\mathrm{d}y}\bigg|_{y=-1} - \epsilon \frac{0.6K\theta_n r S_R}{\beta} U_1(-1) + \text{c.c.} = 0 \tag{3.17a}$$

$$-\frac{Q_{s0} r}{\beta\theta_n^{1/2}} \frac{\mathrm{d}Z_1}{\mathrm{d}y}\bigg|_{y=1} + \epsilon \frac{0.6K\theta_n r S_L}{\beta} U_1(1) + \text{c.c.} = 0 \tag{3.17b}$$

Because the channel center line is $R + L$, the curvature of the channel center line C is written in the form

$$C = \frac{\dfrac{\partial^2 (R+L)}{\partial x^2}}{\left[1 + \left(\dfrac{\partial (R+L)}{\partial x}\right)^2\right]^{3/2}} = -Ak^2(R_1 + L_1)\exp\left[\mathrm{i}(kx - \omega t)\right] + \text{c.c.} \tag{3.18}$$

Because the curvature C is on the order of A as shown above, and $Q_{sR,j}$ and $Q_{sL,j}$ are also on the order of A as shown in (3.14) and (3.15) respectively, the effect of the curvature does not appear in the bank erosion model at the linear level. Expanding the bank erosion model (2.49)–(2.52) with the use of A, we obtain the following relations:

$$-\mathrm{i}\omega R_1 + \epsilon \frac{0.6K\theta_n r S_R}{\beta} U_1(-1) - \frac{\mathrm{i}\omega}{\beta S_R} Z_1(-1) + \text{c.c.} = 0 \tag{3.19}$$

$$-\mathrm{i}\omega L_1 - \epsilon \frac{0.6K\theta_n r S_L}{\beta} U_1(1) + \frac{\mathrm{i}\omega}{\beta S_L} Z_1(1) + \text{c.c.} = 0 \tag{3.20}$$

Combining (3.10), (3.11), (3.19), and (3.20), we can eliminate R_1 and L_1, and obtain the following relations:

$$-\frac{\omega}{k} V_1(-1) - \frac{\mathrm{i}\omega}{\beta S_R} Z_1(-1) + \epsilon \frac{0.6K\theta_n r S_R}{\beta} U_1(-1) + \text{c.c.} = 0 \tag{3.21}$$

$$-\frac{\omega}{k} V_1(1) + \frac{\mathrm{i}\omega}{\beta S_L} Z_1(1) - \epsilon \frac{0.6K\theta_n r S_L}{\beta} U_1(1) + \text{c.c.} = 0 \tag{3.22}$$

3.2 Solution

The problem to be solved is the differential system composed of the four differential equations (3.2)–(3.5), and the four boundary conditions (3.16), (3.17), (3.21), and (3.22). The differential system includes the second derivative of Z_1, and the first derivative of V_1 and H_1, and therefore, can be solved with the four boundary conditions.

Recasting the equations, we have

$$a_1 U_1(y) + a_2 H_1(y) + a_3 Z_1(y) = 0 \tag{3.2}$$

$$a_4 V_1(y) + a_5 \frac{\mathrm{d}H_1}{\mathrm{d}y} + a_5 \frac{\mathrm{d}Z_1}{\mathrm{d}y} = 0 \tag{3.3}$$

$$a_6 U_1(y) + \frac{\mathrm{d}V_1}{\mathrm{d}y} + a_6 H_1(y) = 0 \tag{3.4}$$

$$-\mathrm{i}\omega Z_1 + a_7 U_1(y) + a_8 \frac{\mathrm{d}V_1}{\mathrm{d}y} + a_9 \frac{\mathrm{d}^2 Z_1}{\mathrm{d}y^2} = 0 \tag{3.5}$$

$$-\frac{Q_{s0} r}{\beta \theta_n^{1/2}} \frac{\mathrm{d}Z_1}{\mathrm{d}y}\bigg|_{y=-1} - \epsilon \frac{0.6 K \theta_n r S_R}{\beta} U_1(-1) + \text{c.c.} = 0 \tag{3.16}$$

$$-\frac{Q_{s0} r}{\beta \theta_n^{1/2}} \frac{\mathrm{d}Z_1}{\mathrm{d}y}\bigg|_{y=1} + \epsilon \frac{0.6 K \theta_n r S_L}{\beta} U_1(1) + \text{c.c.} = 0 \tag{3.17}$$

$$-\frac{\omega}{k} V_1(-1) - \frac{\mathrm{i}\omega}{\beta S_R} Z_1(-1) + \epsilon \frac{0.6 K \theta_n r S_R}{\beta} U_1(-1) + \text{c.c.} = 0 \tag{3.21}$$

$$-\frac{\omega}{k} V_1(1) + \frac{\mathrm{i}\omega}{\beta S_L} Z_1(1) - \epsilon \frac{0.6 K \theta_n r S_L}{\beta} U_1(1) + \text{c.c.} = 0 \tag{3.22}$$

In addition, we recast (3.10) and (3.11) to clarify the relation between bed geometry and bank geometry. They are

$$\mathrm{i}kR_1 - V_1(-1) + \text{c.c.} = 0 \tag{3.10}$$

$$\mathrm{i}kL_1 - V_1(1) + \text{c.c.} = 0 \tag{3.11}$$

The differential equations (3.2)–(3.5) are linear differential equations with constant coefficients, and therefore, the solutions can be written in the exponential form in general. In this particular case, the solutions are expected to be periodic in the lateral direction. Thus, the exponents should be complex numbers. This means that the solutions can be expressed by sinusoidal functions. From the form of differential system, we find that V_1 is out of phase with the others by π. With this in mind, we find that the following two cases are possible.

1. Case of both banks being in phase

$$(U_1, H_1, Z_1) = (u, h, z)\sin\alpha y + \text{c.c.}, \quad V_1 = v\cos\alpha y + \text{c.c.} \tag{3.23a}$$

In this case V_1 is symmetrical with respect to the x axis, so that it is found that $R_1 = L_1$ from (3.10) and (3.11).

2. Case of both banks being out of phase

$$(U_1, H_1, Z_1) = (u, h, z)\cos\alpha y + \text{c.c.}, \quad V_1 = v\sin\alpha y + \text{c.c.} \tag{3.23b}$$

In this case, V_1 is symmetrical with respect to the origin, so that $R_1 = -L_1$. Therefore, the both banks are out of phase.

Let us think the case of the both banks being in phase.

Substituting (3.23a) into (3.2)–(3.5), we obtain the equations of the form

$$a_1 u + a_2 h + a_3 z = 0 \tag{3.24}$$

$$a_4 v + a_5 \alpha h + a_5 \alpha z = 0 \tag{3.25}$$

$$a_6 u - \alpha v + a_6 h = 0 \tag{3.26}$$

$$a_7 u - a_8 \alpha v + \left(-a_9\alpha^2 - \mathrm{i}\omega\right) z = 0 \tag{3.27}$$

Eqs. (3.24)–(3.26) can be rewritten in the following matrix form:

$$\mathbf{L}(\alpha)\cdot\boldsymbol{u} = \boldsymbol{r}(\alpha) z \tag{3.28a}$$

where

$$\mathbf{L}(\alpha) = \begin{bmatrix} a_1 & 0 & a_2 \\ 0 & a_4 & a_5\alpha \\ a_6 & -\alpha & a_6 \end{bmatrix} \tag{3.28b}$$

$$\boldsymbol{r}(\alpha) = \begin{bmatrix} -a_3 \\ -a_5\alpha \\ 0 \end{bmatrix}, \quad \boldsymbol{u} = \begin{bmatrix} u \\ v \\ h \end{bmatrix} \tag{3.28c, d}$$

Solving (3.28) for $\boldsymbol{u}$, we obtain the following solutions:

$$\begin{bmatrix} u \\ v \\ h \end{bmatrix} = \begin{bmatrix} f_u(\alpha) \\ f_v(\alpha) \\ f_h(\alpha) \end{bmatrix} z \tag{3.29a}$$

where

$$\begin{bmatrix} f_u(\alpha) \\ f_v(\alpha) \\ f_h(\alpha) \end{bmatrix} = \mathbf{L}^{-1}(\alpha)\cdot\boldsymbol{r}(\alpha) = \begin{bmatrix} \dfrac{(a_2 - a_3)a_5\alpha^2 - a_3 a_4 a_6}{(a_1 - a_2)a_4 a_6 + a_1 a_5 \alpha^2} \\ \dfrac{(a_2 - a_1 - a_3)a_5 a_6 \alpha}{(a_1 - a_2)a_4 a_6 + a_1 a_5 \alpha^2} \\ \dfrac{-a_1 a_5 \alpha^2 + a_3 a_4 a_6}{(a_1 - a_2)a_4 a_6 + a_1 a_5 \alpha^2} \end{bmatrix}$$

$$= \begin{bmatrix} \dfrac{\mathrm{i}\beta C_f(k^2-\alpha^2)-k^3}{k^3(F^2-1)-k\alpha^2-\mathrm{i}\beta C_f[(4F^2-1)k^2-2\alpha^2]-3k\beta^2C_f^2F^2} \\ \dfrac{k\alpha(\mathrm{i}k+3\beta C_f)}{k^3(F^2-1)-k\alpha^2-\mathrm{i}\beta C_f[(4F^2-1)k^2-2\alpha^2]-3k\beta^2C_f^2F^2} \\ \dfrac{k(k^2+\alpha^2)-\mathrm{i}\beta C_f(k^2+2\alpha^2)}{k^3(F^2-1)-k\alpha^2-\mathrm{i}\beta C_f[(4F^2-1)k^2-2\alpha^2]-3k\beta^2C_f^2F^2} \end{bmatrix} \tag{3.29b}$$

Note that $f_u(\alpha)$ and $f_h(\alpha)$ are even functions of α while $f_v(\alpha)$ is an odd function of α. Thus, we have U_1, V_1, H_1 and Z_1 in the form

$$\begin{bmatrix} U_1 \\ H_1 \\ Z_1 \end{bmatrix} = \begin{bmatrix} f_u(\alpha) \\ f_h(\alpha) \\ 1 \end{bmatrix} z\sin\alpha y + \text{c.c.} \tag{3.30a}$$

$$V_1 = f_v(\alpha)\, z\cos\alpha y + \text{c.c.} \tag{3.30b}$$

Substituting (3.30) into (3.27), we obtain

$$a_7 f_u(\alpha) z\sin\alpha y - \alpha a_7 f_v(\alpha) z\sin\alpha y + \left(-\alpha^2 a_9 - \mathrm{i}\omega\right) z\sin\alpha y = 0 \tag{3.31}$$

The above equation reduces to

$$\mathcal{A}\alpha^4 + \mathcal{B}\alpha^2 + \mathcal{C} = 0 \tag{3.32a}$$

where

$$\mathcal{A} = a_1 a_5 a_9, \tag{3.32b}$$

$$\mathcal{B} = \mathrm{i}\omega a_1 a_5 - (a_2 - a_3)a_5 a_7 - (a_1 - a_2 + a_3)a_5 a_6 a_8 + (a_1 - a_2)a_4 a_6 a_9, \tag{3.32c}$$

$$\mathcal{C} = \mathrm{i}\omega(a_1 - a_2)a_4 a_6 + a_3 a_4 a_6 a_7 \tag{3.32d}$$

Eqn. (3.32) is the fourth order algebraic equation, which has the four solutions. Solving (3.32) for α, we obtain

$$\alpha = \pm\alpha_a, \pm\alpha_b \tag{3.33a}$$

where

$$\alpha_a = \sqrt{\frac{-\mathcal{B}+\sqrt{\mathcal{B}^2-4\mathcal{A}\mathcal{C}}}{2\mathcal{A}}}, \quad \alpha_b = \sqrt{\frac{-\mathcal{B}-\sqrt{\mathcal{B}^2-4\mathcal{A}\mathcal{C}}}{2\mathcal{A}}}, \tag{3.33b, c}$$

With the use of α_a and α_b, the solutions can be written in the form of the linear combination of linearly independent solutions, such that

$$\begin{aligned} U_1 = {} & f_u(\alpha_a)\, z_{1,a}^{+}\sin\alpha_a y + f_u(-\alpha_a)\, z_{1,a}^{-}\sin(-\alpha_a y) \\ & + f_u(\alpha_b)\, z_{1,b}^{+}\sin\alpha_b y + f_u(-\alpha_b)\, z_{1,b}^{-}\sin(-\alpha_b y) + \text{c.c.} \end{aligned} \tag{3.34a}$$

$$V_1 = f_v(\alpha_a)\, z^+_{1,a} \cos\alpha_a y + f_v(-\alpha_a)\, z^-_{1,a} \cos(-\alpha_a y) + f_v(\alpha_b)\, z^+_{1,b} \cos\alpha_b y + f_v(-\alpha_b)\, z^-_{1,b} \cos(-\alpha_b y) + \text{c.c.} \quad (3.34b)$$

$$H_1 = f_h(\alpha_a) z^+_{1,a} \sin\alpha_a y + f_h(-\alpha_a) z^-_{1,a} \sin(-\alpha_a y) + f_h(\alpha_b)\, z^+_{1,b} \sin\alpha_b y + f_h(-\alpha_b)\, z^-_{1,b} \sin(-\alpha_b y) + \text{c.c.} \quad (3.34c)$$

$$Z_1 = z^+_{1,a} \sin\alpha_a y + z^-_{1,a} \sin(-\alpha_a y) + z^+_{1,b} \sin\alpha_b y + z^-_{1,b} \sin(-\alpha_b y) + \text{c.c.} \quad (3.34d)$$

where $z^+_{1,i}$ and $z^-_{1,i}$ $(i = a, b)$ are the coefficients corresponding to $\alpha_{1,i}$ and $-\alpha_{1,i}$ $(i = a, b)$, respectively. From (3.29), we find that the denominators of $f_u(\alpha)$, $f_v(\alpha)$ and $f_h(\alpha)$, and the numerator of $f_u(\alpha)$ and $f_h(\alpha)$ are all functions of α squared while only the numerator of $f_v(\alpha)$ is proportional to α. Therefore, we have the relation

$$f_u(-\alpha) = f_u(\alpha), \quad f_v(-\alpha) = -f_v(\alpha), \quad f_h(-\alpha) = f_h(\alpha) \quad (3.35)$$

With the above relations in mind, we find that the solutions of (3.2)–(3.5) can be written in the form

$$U_1 = f_u(\alpha_a)\, z_{1,a} \sin\alpha_a y + f_u(\alpha_b)\, z_{1,b} \sin\alpha_b y + \text{c.c.} \quad (3.36a)$$

$$V_1 = f_v(\alpha_a)\, z_{1,a} \cos\alpha_a y + f_v(\alpha_b)\, z_{1,b} \cos\alpha_b y + \text{c.c.} \quad (3.36b)$$

$$H_1 = f_v(\alpha_a)\, z_{1,a} \sin\alpha_a y + f_h(\alpha_b)\, z_{1,b} \sin\alpha_b y + \text{c.c.} \quad (3.36b)$$

$$Z_1 = z_{1,a} \sin\alpha_a y + z_{1,b} \sin\alpha_b y + \text{c.c.} \quad (3.36b)$$

where $z_{1,i} = z^+_{1,i} - z^-_{1,i}$ $(i = a, b)$. The above solutions have to satisfy the boundary conditions from (3.16) to (3.22). Substituting (3.35), (3.16) and (3.17) reduce to the following single equation:

$$\frac{rQ_{s0}}{\beta\theta_n^{1/2}} (\alpha_a z_{1,a} \cos\alpha_a - \alpha_b z_{1,b} \cos\alpha_b) - \epsilon \frac{0.6K\theta_n r S_B}{\beta} [f_u(\alpha_a)\, z_{1,a} \sin\alpha_a + f_u(\alpha_b)\, z_{1,b} \sin\alpha_b] + \text{c.c.} \quad (3.37)$$

where the lateral slopes of both banks are assumed to be identical, and denoted by S_B. This practice is followed hereafter. Similarly, (3.21) and (3.22) reduce to

$$-\frac{\omega}{k} [f_v(\alpha_a)\, z_{1,a} \cos\alpha_a + f_v(\alpha_b)\, z_{1,b} \cos\alpha_b] + \frac{\mathrm{i}\omega}{\beta S_B} (z_{1,a} \sin\alpha_a + z_{1,b} \sin\alpha_b) - \epsilon \frac{0.6K\theta_n r S_B}{\beta} [f_u(\alpha_a)\, z_{1,a} \sin\alpha_a + f_u(\alpha_b)\, z_{1,b} \sin\alpha_b] + \text{c.c.} = 0 \quad (3.38)$$

The above two equations can be rewritten in the following matrix form:

$$\begin{bmatrix} l_{11} & l_{12} \\ l_{21} & l_{22} \end{bmatrix} \begin{bmatrix} z_{1,a} \\ z_{1,b} \end{bmatrix} = 0 \tag{3.39a}$$

where

$$l_{11} = -\frac{rQ_{s0}}{\beta\theta_n^{1/2}}\alpha_a \cos\alpha_a + \epsilon\frac{0.6K\theta_n rS_B}{\beta} f_u(\alpha_a)\sin\alpha_a, \tag{3.39b}$$

$$l_{12} = -\frac{\omega}{k} f_v(\alpha_a)\cos\alpha_a + \left(\frac{\mathrm{i}\omega}{\beta S_B} - \epsilon\frac{0.6K\theta_n rS_B}{\beta} f_u(\alpha_a)\right)\sin\alpha_a, \tag{3.39c}$$

$$l_{21} = -\frac{rQ_{s0}}{\beta\theta_n^{1/2}}\alpha_b \cos\alpha_b + \epsilon\frac{0.6K\theta_n rS_B}{\beta} f_u(\alpha_b)\sin\alpha_b, \tag{3.39d}$$

$$l_{22} = -\frac{\omega}{k} f_v(\alpha_b)\cos\alpha_b + \left(\frac{\mathrm{i}\omega}{\beta S_B} - \epsilon\frac{0.6K\theta_n rS_B}{\beta} f_u(\alpha_b)\right)\sin\alpha_b, \tag{3.39f}$$

The solvability condition for (3.39) is the following:

$$|l_{ij}| = l_{11}l_{22} - l_{12}l_{21} = 0 \tag{3.40}$$

The above equation includes ω, k, β and other parameters. Solving (3.39), we can obtain ω as a function of k, β and other parameters. However, (3.39) is not easy to solve. We employ an approximate method. Assuming that ϵ is small, we solve the problem with the use of the expansions of ϵ, hereafter. The small parameter ϵ is a coefficient reflecting the bank protection from erosion. When ϵ is unity, there is no bank protection while, when ϵ vanishes, there is no bank erosion at all. Therefore, when ϵ vanishes, the problem is expected to reduce to the bar instability problem without bank erosion.

3.2.1 ϵ expansion

As described earlier, in order to keep the total channel width constant, ϵ should be rather small. With this in mind, we introduce the expansions with the use of the small parameter ϵ. All the variables are expanded in the form

$$(U_1, V_1, H_1, Z_1) = (U_{10}, V_{10}, H_{10}, Z_{10}) + \epsilon\,(U_{11}, V_{11}, H_{11}, Z_{11}) \tag{3.41}$$

Correspondingly, the complex angular frequency ω is also expanded in the form

$$\omega = \omega_0 + \epsilon\omega_1 \tag{3.42}$$

The case of both banks being in phase

Substituting (3.41) and (3.42) into (3.2)–(3.5), (3.16), (3.17), (3.21), and (3.22), we obtain the following results at each order of ϵ.

At $O(1)$

At $O(1)$, we have

$$a_1 U_{10} + a_2 H_{10} + a_3 Z_{10} = 0 \tag{3.43}$$

$$a_4 V_{10} + a_5 \frac{\mathrm{d}H_{10}}{\mathrm{d}y} + a_5 \frac{\mathrm{d}Z_{10}}{\mathrm{d}y} = 0 \tag{3.44}$$

$$a_6 U_{10} + \frac{\mathrm{d}V_{10}}{\mathrm{d}y} + a_6 H_{10} = 0 \tag{3.45}$$

$$-\mathrm{i}\omega_0 Z_{10} + a_7 U_{10} + a_8 \frac{\mathrm{d}V_{10}}{\mathrm{d}y} + a_9 \frac{\mathrm{d}^2 Z_{10}}{\mathrm{d}y^2} = 0 \tag{3.46}$$

The boundary conditions supplementing the above differential system are

$$\left.\frac{\mathrm{d}Z_{10}}{\mathrm{d}y}\right|_{y=-1} + \text{c.c.} = 0 \tag{3.47}$$

$$\left.\frac{\mathrm{d}Z_{10}}{\mathrm{d}y}\right|_{y=1} + \text{c.c.} = 0 \tag{3.48}$$

$$V_{10}(-1) + \frac{\mathrm{i}k}{\beta S_B} Z_{10}(-1) + \text{c.c.} = 0 \tag{3.49}$$

$$V_{10}(1) - \frac{\mathrm{i}k}{\beta S_B} Z_{10}(1) + \text{c.c.} = 0 \tag{3.50}$$

As already described, the solutions have the form

$$U_{10} = f_u(\alpha_a)\, z_{10,a} \sin \alpha_a y + f_u(\alpha_b)\, z_{10,b} \sin \alpha_b y + \text{c.c.} \tag{3.51}$$

$$V_{10} = f_v(\alpha_a)\, z_{10,a} \cos \alpha_a y + f_v(\alpha_b)\, z_{10,b} \cos \alpha_b y + \text{c.c.} \tag{3.52}$$

$$H_{10} = f_h(\alpha_a)\, z_{10,a} \sin \alpha_a y + f_h(\alpha_b)\, z_{10,b} \sin \alpha_b y + \text{c.c.} \tag{3.53}$$

$$Z_{10} = z_{10,a} \sin \alpha_a y + z_{10,b} \sin \alpha_b y + \text{c.c.} \tag{3.54}$$

Assuming that $z_{10,i}$ and α_i $(i = a, b)$ to be real, we find Z_{10} real, and therefore, we find from (3.47) and (3.48) that the following condition has to be satisfied:

$$\alpha_a z_{10,a} \cos \alpha_a + \alpha_b z_{10,b} \cos \alpha_b = 0 \tag{3.55}$$

In addition, we find from (3.49) and (3.50) that the real part of $V_{10}(\pm 1)$ has to vanish. Therefore, the following condition should be satisfied:

$$\mathrm{Re}[V_{10}(\pm 1)] = \mathrm{Re}[f_v(\alpha_a)] z_{10,a} \cos\alpha_a + \mathrm{Re}[f_v(\alpha_b)] z_{10,b} \cos\alpha_b = 0 \tag{3.56}$$

The above conditions are satisfied if either of α_a or α_b is $(m+1/2)\pi$ ($m = 0, 1, 2, 3\cdots$), and the coefficient of the other α vanishes. We assume that $\alpha_a = (m+1/2)\pi$ ($m = 0, 1, 2, 3\cdots$). That is

$$\alpha_{a,m} = \left(m + \frac{1}{2}\right)\pi \quad (m = 0, 1, 2, 3\cdots) \quad \text{and} \quad z_{10,b,m} = 0 \tag{3.57}$$

where $\alpha_{a,m} = (m+1/2)\pi$, and $z_{10,b,m}$ is the coefficient corresponding to $\alpha_{b,m}$, which can be obtained from the following relation:

$$\alpha_{10,b,m} = \sqrt{-\frac{\mathcal{B}}{\mathcal{A}} - \alpha_{10,a,m}^2} \tag{3.58}$$

where $\mathcal{A}$ is given by (3.32b), and $\mathcal{B}$ is (3.32c) with ω replaced by ω_0. The solutions are, then, written in the form

$$U_{10} = f_u(\alpha_{a,m})\ z_{10,a,m} \sin\alpha_{a,m} y \tag{3.59a}$$

$$V_{10} = f_v(\alpha_{a,m})\ z_{10,a,m} \cos\alpha_{a,m} y \tag{3.59b}$$

$$H_{10} = f_h(\alpha_{a,m})\ z_{10,a,m} \sin\alpha_{a,m} y \tag{3.59c}$$

$$Z_{10} = z_{10,a,m} \sin\alpha_{a,m} y \tag{3.59d}$$

where $z_{10,a,m}$ is the coefficient corresponding to $\alpha_{a,m}$.

Substituting (3.59) into (3.46), we have

$$-\mathrm{i}\omega_0 + a_7 f_u(\alpha_{a,m}) + a_8 \alpha_{a,m} f_v(\alpha_{a,m}) + a_9 \alpha_{a,m}^2 = 0 \tag{3.60}$$

Denoting ω_0 corresponding to $\alpha_{a,m}$ by $\omega_{0,m}$, we obtain

$$\omega_{0,m} = -\mathrm{i}\left[a_7 f_u(\alpha_{a,m}) + a_8 \alpha_{a,m} f_v(\alpha_{a,m}) + a_9 \alpha_{a,m}^2\right] \tag{3.61}$$

At $O(\epsilon)$

At $O(\epsilon)$, we have

$$a_1 U_{11} + a_2 H_{11} + a_3 Z_{11} = 0 \tag{3.62}$$

$$a_4 V_{11} + a_5 \frac{\mathrm{d}H_{11}}{\mathrm{d}y} + a_5 \frac{\mathrm{d}Z_{11}}{\mathrm{d}y} = 0 \tag{3.63}$$

$$a_6 U_{11} + \frac{\mathrm{d}V_{11}}{\mathrm{d}y} + a_6 H_{11} = 0 \tag{3.64}$$

$$-\mathrm{i}\omega_0 Z_{11} + a_7 U_{11} + a_8 \frac{\mathrm{d}V_{11}}{\mathrm{d}y} + a_9 \frac{\mathrm{d}^2 Z_{11}}{\mathrm{d}y^2} = \mathrm{i}\omega_1 Z_{10} \tag{3.65}$$

It is found that the the above equations have the same form as (3.43)–(3.46) except for the right hand side of (3.65), which includes the solution of (3.43)–(3.46). That is, the homogeneous parts of (3.62)–(3.65) are identical to those of (3.43)–(3.46), (3.64) has an inhomogeneous term including the solution of (3.43)–(3.46). In such a case, the solutions of (3.62)–(3.65) consist of two parts: homogeneous solutions satisfying the homogeneous equations (3.62)–(3.65) with dropping the right hand side of (3.65), and inhomogeneous solutions satisfying the whole equations. Because the inhomogeneous term of (3.65) has the form of $\sin\alpha_{a,m}y$, the inhomogeneous solutions should have the form of $y\cos\alpha_{a,m}y$ and $y\sin\alpha_{a,m}y$. The general solutions, then, take the form

$$U_{11} = u^{(h)}_{11,a,m}\sin\alpha_{a,m}y + u^{(h)}_{11,b,m}\sin\alpha_{b,m}y + u^{(i)}_{11,a,m}y\cos\alpha_{a,m}y \tag{3.66}$$

$$V_{11} = v^{(h)}_{11,a,m}\cos\alpha_{a,m}y + v^{(h)}_{11,b,m}\cos\alpha_{b,m}y + v^{(i)}_{11,a,m}y\sin\alpha_{a,m}y \tag{3.67}$$

$$H_{11} = h^{(h)}_{11,a,m}\sin\alpha_{a,m}y + h^{(h)}_{11,b,m}\sin\alpha_{b,m}y + h^{(i)}_{11,m}y\cos\alpha_{a,m}y \tag{3.68}$$

$$Z_{11} = z^{(h)}_{11,a,m}\sin\alpha_{a,m}y + z^{(h)}_{11,b,m}\sin\alpha_{b,m}y + z^{(i)}_{11,a,m}y\cos\alpha_{a,m}y \tag{3.69}$$

Substituting the above solutions into (3.62)–(3.64), we obtain

$$\begin{aligned} a_1 u^{(h)}_{11,a,m}\sin\alpha_{a,m}y \;&+\; a_1 u^{(h)}_{11,b,m}\sin\alpha_{b,m}y + a_1 u^{(i)}_{11,a,m}y\cos\alpha_{a,m}y \\ &+\; a_2 h^{(h)}_{11,a,m}\sin\alpha_{a,m}y + a_2 h^{(h)}_{11,b,m}\sin\alpha_{b,m}y + a_2 h^{(i)}_{11,a,m}y\cos\alpha_{a,m}y \\ &+\; a_3 z^{(h)}_{11,a,m}\sin\alpha_{a,m}y + a_3 z^{(h)}_{11,b,m}\sin\alpha_{b,m}y + a_3 z^{(i)}_{11,a,m}y\cos\alpha_{a,m}y = 0 \end{aligned} \tag{3.70}$$

$$\begin{aligned} a_4 v^{(h)}_{11,a,m}\cos\alpha_{a,m}y \;&+\; a_4 v^{(h)}_{11,b,m}\cos\alpha_{b,m}y + a_4 v^{(i)}_{11,a,m}y\sin\alpha_{a,m}y \\ &+\; a_5\alpha_{a,m}h^{(h)}_{11,a,m}\cos\alpha_{a,m}y + a_5\alpha_{b,m}h^{(h)}_{11,b,m}\cos\alpha_{b,m}y \\ &\qquad + a_5 h^{(i)}_{11,a,m}\cos\alpha_{a,m}y - a_5\alpha_{a,m}h^{(i)}_{11,a,m}y\sin\alpha_{a,m}y \\ &+\; a_5\alpha_{a,m}z^{(h)}_{11,a,m}\cos\alpha_{a,m}y + a_5\alpha_{b,m}z^{(h)}_{11,b,m}\cos\alpha_{b,m}y \\ &\qquad + a_5 z^{(i)}_{11,a,m}\cos\alpha_{a,m}y - a_5\alpha_{a,m}z^{(i)}_{11,a,m}y\sin\alpha_{a,m}y = 0 \end{aligned} \tag{3.71}$$

$$
\begin{aligned}
a_6 u^{(h)}_{11,a,m} \sin\alpha_{a,m} y \quad &+ \quad a_6 u^{(h)}_{11,b,m} \sin\alpha_{b,m} y + a_6 u^{(i)}_{11,a,m} y \cos\alpha_{a,m} y \\
&- \quad \alpha_{a,m} v^{(h)}_{11,a,m} \sin\alpha_{a,m} y - \alpha_{b,m} v^{(i)}_{11,b,m} \sin\alpha_{b,m} y \\
&\qquad + v^{(i)}_{11,a,m} \sin\alpha_{a,m} y + \alpha_{a,m} v, 11, a, m^{(i)} y \cos\alpha_{a,m} y \\
&+ \quad a_6 h^{(h)}_{11,a,m} \sin\alpha_{a,m} y + a_6 h^{(h)}_{11,b,m} \sin\alpha_{b,m} y + a_6 h^{(i)}_{11,a,m} y \cos\alpha_{a,m} y = 0
\end{aligned}
\tag{3.72}
$$

Collecting terms including $\sin\alpha_{a,m} y$ and $\cos\alpha_{a,m} y$ in the above equations, we obtain

$$
\begin{aligned}
a_1 u^{(h)}_{11,a,m} + a_2 h^{(h)}_{11,a,m} &= -a_3 z^{(h)}_{11,a,m} && (3.73)\\
a_4 v^{(h)}_{11,a,m} + a_5 \alpha_{a,m} h^{(h)}_{11,a,m} &= -a_5 \alpha_{a,m} z^{(h)}_{11,a,m} \\
&\qquad -a_5 \alpha_{a,m} \left(h^{(i)}_{11,a,m} + z^{(i)}_{11,a,m} \right) && (3.74)\\
a_6 u^{(h)}_{11,a,m} + \alpha_{a,m} v^{(h)}_{11,a,m} + a_6 h^{(h)}_{11,a,m} &= -\alpha_m v^{(i)}_{11,a,m} && (3.75)
\end{aligned}
$$

Collecting terms including $\sin\alpha_{b,m} y$ and $\cos\alpha_{b,m} y$ in the above equations, we obtain

$$
\begin{aligned}
a_1 u^{(h)}_{11,b,m} + a_2 h^{(h)}_{11,b,m} &= -a_3 z^{(h)}_{11,b,m} && (3.76)\\
a_4 v^{(h)}_{11,b,m} + a_5 \alpha_{b,m} h^{(h)}_{11,b,m} &= -a_5 \alpha_{b,m} z^{(h)}_{11,b,m} && (3.77)\\
a_6 u^{(h)}_{11,b,m} + \alpha_{b,m} v^{(h)}_{11,b,m} + a_6 h^{(h)}_{11,b,m} &= 0 && (3.78)
\end{aligned}
$$

Collecting terms including $y \sin\alpha_m y$ and $y \cos\alpha_m y$ in (3.70)–(3.72), we obtain

$$
\begin{aligned}
a_1 u^{(i)}_{11,a,m} + a_2 h^{(i)}_{11,a,m} &= -a_3 z^{(i)}_{11,a,m} && (3.79)\\
a_4 v^{(i)}_{11,a,m} + a_5 \alpha_{a,m} h^{(i)}_{11,a,m} &= -a_5 \alpha_{a,m} z^{(i)}_{11,a,m} && (3.80)\\
a_6 u^{(i)}_{11,a,m} + \alpha_{a,m} v^{(i)}_{11,a,m} + a_6 h^{(i)}_{11,a,m} &= 0 && (3.81)
\end{aligned}
$$

Eqs. (3.73)–(3.75) can be written in the following matrix form:

$$
\mathbf{L}(\alpha_{a,m}) \cdot \begin{bmatrix} u^{(h)}_{11,a,m} \\ v^{(h)}_{11,a,m} \\ h^{(h)}_{11,a,m} \end{bmatrix} = \boldsymbol{r}(\alpha_{a,m}) z^{(h)}_{11,a,m} + \begin{bmatrix} 0 \\ -a_5 (h^{(i)}_{11,a,m} + z^{(i)}_{11,a,m}) \\ -\alpha_m v^{(i)}_{11,a,m} \end{bmatrix} \tag{3.82}
$$

Eqs. (3.76)–(3.78) can be written in the following matrix form:

$$
\mathbf{L}(\alpha_{b,m}) \cdot \begin{bmatrix} u^{(h)}_{11,b,m} \\ v^{(h)}_{11,b,m} \\ h^{(h)}_{11,b,m} \end{bmatrix} = \boldsymbol{r}(\alpha_{b,m}) z^{(h)}_{11,b,m} \tag{3.83}
$$

Eqs. (3.79)–(3.81) can be written in the form

$$\mathbf{L}(\alpha_{a,m}) \cdot \begin{bmatrix} u^{(i)}_{11,a,m} \\ v^{(i)}_{11,a,m} \\ h^{(i)}_{11,a,m} \end{bmatrix} = \boldsymbol{r}(\alpha_m) z^{(i)}_{11,a,m} \tag{3.84}$$

The solution of (3.82) is

$$\begin{bmatrix} u^{(h)}_{11,a,m} \\ v^{(h)}_{11,a,m} \\ h^{(h)}_{11,a,m} \end{bmatrix} = \begin{bmatrix} f_u(\alpha_{a,m}) \\ f_v(\alpha_{a,m}) \\ f_h(\alpha_{a,m}) \end{bmatrix} z^{(h)}_{11,a,m} + \begin{bmatrix} g_u(\alpha_{a,m}) \\ g_v(\alpha_{a,m}) \\ g_h(\alpha_{a,m}) \end{bmatrix} z^{(i)}_{11,a,m} \tag{3.85}$$

where

$$\begin{bmatrix} g_u(\alpha_{a,m}) \\ g_v(\alpha_{a,m}) \\ g_h(\alpha_{a,m}) \end{bmatrix} = \mathbf{L}^{-1}(\alpha_{a,m}) \begin{bmatrix} 0 \\ -a_5 \left(f_h(\alpha_{a,m}) + 1\right) \\ -\alpha_m f_v(\alpha_{a,m}) \end{bmatrix} \tag{3.86}$$

The solution of (3.83) takes the form

$$\begin{bmatrix} u^{(h)}_{11,b,m} \\ v^{(h)}_{11,b,m} \\ h^{(h)}_{11,b,m} \end{bmatrix} = \begin{bmatrix} f_u(\alpha_{b,m}) \\ f_v(\alpha_{b,m}) \\ f_h(\alpha_{b,m}) \end{bmatrix} z^{(h)}_{11,b,m} \tag{3.87}$$

The solution of (3.84) takes the form

$$\begin{bmatrix} u^{(i)}_{11,a,m} \\ v^{(i)}_{11,a,m} \\ h^{(i)}_{11,a,m} \end{bmatrix} = \begin{bmatrix} f_u(\alpha_{a,m}) \\ f_v(\alpha_{a,m}) \\ f_h(\alpha_{a,m}) \end{bmatrix} z^{(i)}_{11,a,m} \tag{3.88}$$

The solutions of (3.66)–(3.69) can be written in the form

$$\begin{aligned} U_{11} = [f_u(\alpha_{a,m})\, z^{(h)}_{11,a,m} \;&+\; g_u(\alpha_{a,m})\, z^{(i)}_{11,a,m}] \sin \alpha_{a,m} y \\ &+\; f_u(\alpha_{b,m})\, z^{(h)}_{11,b,m} \sin \alpha_{b,m} y + f_u(\alpha_{a,m})\, z^{(i)}_{11,a,m} y \cos \alpha_{a,m} y \end{aligned} \tag{3.89}$$

$$\begin{aligned} V_{11} = [f_v(\alpha_{a,m})\, z^{(h)}_{11,a,m} \;&+\; g_v(\alpha_{a,m})\, z^{(i)}_{11,a,m}] \cos \alpha_{a,m} y \\ &+\; f_v(\alpha_{b,m})\, z^{(h)}_{11,b,m} \cos \alpha_{b,m} y + f_v(\alpha_{a,m})\, z^{(i)}_{11,a,m} y \sin \alpha_{a,m} y \end{aligned} \tag{3.90}$$

$$\begin{aligned} H_{11} = [f_h(\alpha_{a,m})\, z^{(h)}_{11,a,m} \;&+\; g_h(\alpha_{a,m})\, z^{(i)}_{11,a,m}] \sin \alpha_{a,m} y \\ &+\; f_h(\alpha_{b,m})\, z^{(h)}_{11,b,m} \sin \alpha_{b,m} y + f_h(\alpha_{a,m})\, z^{(i)}_{11,a,m} y \cos \alpha_{a,m} y \end{aligned} \tag{3.91}$$

$$Z_{11} = z^{(h)}_{11,a,m} \sin \alpha_{a,m} y + z^{(h)}_{11,b,m} \sin \alpha_{b,m} y + z^{(i)}_{11,a,m} y \cos \alpha_{a,m} y \tag{3.92}$$

The coefficient $z^{(h)}_{11,a,m}$, $z^{(h)}_{11,b,m}$ and $z^{(i)}_{11,a,m}$ are determined by the following boundary condition at $O(\epsilon)$:

$$-\frac{Q_{s0} r}{\beta \theta_n^{1/2}} \left. \frac{\mathrm{d}Z_{11}}{\mathrm{d}y} \right|_{y=-1} - \frac{0.6 K \theta_n r S_B}{\beta} U_{10}(-1) + \text{c.c.} = 0 \tag{3.93}$$

$$-\frac{Q_{s0} r}{\beta \theta_n^{1/2}} \left. \frac{\mathrm{d}Z_{11}}{\mathrm{d}y} \right|_{y=1} + \frac{0.6 K \theta_n r S_B}{\beta} U_{10}(1) + \text{c.c.} = 0 \tag{3.94}$$

$$-\omega_1 \left[\frac{V_{10}(-1)}{k} + \mathrm{i} \frac{Z_{10}(-1)}{\beta S_B} \right] - \omega_0 \left[\frac{V_{11}(-1)}{k} + \mathrm{i} \frac{Z_{11}(-1)}{\beta S_B} \right] + \frac{0.6 K \theta_n r S_B}{\beta} U_{10}(-1) + \text{c.c.} = 0 \tag{3.95}$$

$$-\omega_1 \left[\frac{V_{10}(1)}{k} - \mathrm{i} \frac{Z_{10}(1)}{\beta S_B} \right] + \omega_0 \left[\frac{V_{11}(1)}{k} - \mathrm{i} \frac{Z_{11}(1)}{\beta S_B} \right] - \frac{0.6 K \theta_n r S_B}{\beta} U_{10}(1) + \text{c.c.} = 0 \tag{3.96}$$

Substituting (3.89)–(3.91) into (3.93) and (3.94), we obtain the same equation of the form

$$-\frac{Q_{s0} r}{\beta \theta_n^{1/2}} \left(\alpha_{a,m} z^{(h)}_{11,a,m} \cos \alpha_{a,m} + \alpha_{b,m} z^{(h)}_{11,b,m} \cos \alpha_{b,m} + z^{(i)}_{11,a,m} \cos \alpha_{a,m} - \alpha_{a,m} z^{(i)}_{11,a,m} \sin \alpha_{a,m} \right) + \frac{0.6 K \theta_n r S_B}{\beta} f_u(\alpha_{a,m}) z_{10,a,m} \sin \alpha_{a,m} + \text{c.c.} = 0 \tag{3.97}$$

Because $\cos \alpha_{a,m} = 0$, and $\sin \alpha_{a,m} = 1$ when m is even, and $\sin \alpha_{a,m} = -1$ when m is odd, the above equation is reduced to

$$\frac{Q_{s0} r}{\beta \theta_n^{1/2}} \left(\alpha_{b,m} z^{(h)}_{11,b,m} \cos \alpha_{b,m} - \alpha_{a,m} z^{(i)}_{11,a,m} \right) - \frac{0.6 K \theta_n r S_B}{\beta} f_u(\alpha_{a,m})\, z_{10,m} + \text{c.c.} = 0 \quad \text{when} \quad m = \text{even} \tag{3.98a}$$

$$\frac{Q_{s0} r}{\beta \theta_n^{1/2}} \left(\alpha_{b,m} z^{(h)}_{11,b,m} \cos \alpha_{b,m} + \alpha_{a,m} z^{(i)}_{11,a,m} \right) + \frac{0.6 K \theta_n r S_B}{\beta} f_u(\alpha_{a,m})\, z_{10,m} + \text{c.c.} = 0 \quad \text{when} \quad m = \text{odd} \tag{3.98b}$$

From (3.95) and (3.96), we obtain

$$\omega_1 \left(\frac{1}{k} f_v(\alpha_{a,m})\, z_{10,a,m} \cos \alpha_{a,m} - \frac{\mathrm{i}}{\beta S_B} z_{10,a,m} \sin \alpha_{a,m} \right)$$

$$+\omega_0\Big[\frac{1}{k}\Big(f_v(\alpha_{a,m})\,z^{(h)}_{11,a,m}\cos\alpha_{a,m}+g_v(\alpha_{a,m})\,z^{(i)}_{11,a,m}\cos\alpha_{a,m}+f_v(\alpha_{b,m})\,z^{(h)}_{11,b,m}\cos\alpha_{b,m}$$
$$+f_v(\alpha_{a,m})\,z^{(i)}_{11,a,m}\sin\alpha_{a,m}\Big)$$
$$-\frac{\mathrm{i}}{\beta S_B}\Big(z^{(h)}_{11,a,m}\sin\alpha_{a,m}+z^{(h)}_{11,b,m}\sin\alpha_{b,m}+z^{(i)}_{11,a,m}\cos\alpha_{a,m}\Big)\Big]$$
$$+\frac{0.6K\theta_n r S_B}{\beta}f_u(\alpha_{a,m})\,z_{10,a,m}\sin\alpha_{a,m}+\text{c.c.}=0 \tag{3.99}$$

Again, because $\cos\alpha_{a,m}=0$, and $\sin\alpha_{a,m}=1$ when m is even, and $\sin\alpha_{a,m}=-1$ when m is odd, the above equation is reduced to

$$\frac{\omega_0}{k}\Big(f_v(\alpha_{b,m})\,z^{(h)}_{11,b,m}\cos\alpha_{b,m}+f_v(\alpha_{a,m})\,z^{(i)}_{11,a,m}\Big)$$
$$+\frac{0.6K\theta_n r S_B}{\beta}f_u(\alpha_{a,m})\,z_{10,a,m}+\text{c.c.}=0\quad\text{when}\quad m=\text{even} \tag{3.100a}$$
$$\frac{\omega_0}{k}\Big(f_v(\alpha_{b,m})\,z^{(h)}_{11,b,m}\cos\alpha_{b,m}-f_v(\alpha_{a,m})\,z^{(i)}_{11,a,m}\Big)$$
$$-\frac{0.6K\theta_n r S_B}{\beta}f_u(\alpha_{a,m})\,z_{10,a,m}+\text{c.c.}=0\quad\text{when}\quad m=\text{odd} \tag{3.100b}$$

From (3.98a) and (3.100a), we obtain

$$\begin{bmatrix}\dfrac{Q_{s0}r}{\beta\theta_n^{1/2}}\alpha_{b,m}\cos\alpha_{b,m} & -\dfrac{Q_{s0}r}{\beta\theta_n^{1/2}}\alpha_{a,m}\\ \dfrac{\omega_0}{k}f_v(\alpha_{b,m})\cos\alpha_{b,m} & \dfrac{\omega_0}{k}f_v(\alpha_{a,m})\end{bmatrix}\begin{bmatrix}z^{(h)}_{11,b,m}\\ z^{(i)}_{11,a,m}\end{bmatrix}=\begin{bmatrix}\dfrac{0.6K\theta_n r S_B}{\beta}f_u(\alpha_{a,m})\\ -\dfrac{0.6K\theta_n r S_B}{\beta}f_u(\alpha_{a,m})\end{bmatrix}z_{10,a,m}$$
$$\text{when}\quad m=\text{even} \tag{3.101}$$

From (3.98a) and (3.100a), we obtain

$$\begin{bmatrix}\dfrac{Q_{s0}r}{\beta\theta_n^{1/2}}\alpha_{b,m}\cos\alpha_{b,m} & \dfrac{Q_{s0}r}{\beta\theta_n^{1/2}}\alpha_{a,m}\\ \dfrac{\omega_0}{k}f_v(\alpha_{b,m})\cos\alpha_{b,m} & -\dfrac{\omega_0}{k}f_v(\alpha_{a,m})\end{bmatrix}\begin{bmatrix}z^{(h)}_{11,b,m}\\ z^{(i)}_{11,a,m}\end{bmatrix}=\begin{bmatrix}-\dfrac{0.6K\theta_n r S_B}{\beta}f_u(\alpha_{a,m})\\ \dfrac{0.6K\theta_n r S_B}{\beta}\end{bmatrix}z_{10,a,m}$$
$$\text{when}\quad m=\text{even} \tag{3.102}$$

Solving the above equations, we obtain $z^{(h)}_{11,b,m}$, $z^{(i)}_{11,a,m}$ as linear functions of $z_{10,a,m}$.

The above solution is substituted into (3.96) to provide the perturbed angular frequency ω_1.

3.3 Numerical solution

We solve the problem by a numerical scheme called the spectral collocation method with the use of the Chebyshev expansion. We do not use ϵ expansion in this section. We start with the equations (3.2)–(3.5) and (3.16)–(3.22). With the use of the Chebyshev polynomials, the variables can be expanded in the form

$$U_1(y) = \sum_{i=0}^{N} c_i T_i(y) \tag{3.103}$$

$$V_1(y) = \sum_{i=0}^{N} c_{N+1+i} T_i(y) \tag{3.104}$$

$$H_1(y) = \sum_{i=0}^{N} c_{2(N+1)+i} T_i(y) \tag{3.105}$$

$$Z_1(y) = \sum_{i=0}^{N} c_{3(N+1)+i} T_i(y) \tag{3.106}$$

where N is the total number of terms of the Chebyshev polynomials, T_i is the i-th term of the Chebyshev polynomials. By numbering the coefficient c_i in the manner described above, we can use only one kind of coefficient.

Substituting the above equations into (3.2)–(3.5), we obtain

$$a_1 \sum_{i=0}^{N} c_i T_i(y) + a_2 \sum_{i=0}^{N} c_{2(N+1)+i} T_i(y) + a_3 \sum_{i=0}^{N} c_{3(N+1)+i} T_i(y) = 0 \tag{3.107}$$

$$a_4 \sum_{i=0}^{N} c_{N+1+i} T_i(y) + a_5 \sum_{i=0}^{N} c_{2(N+1)+i} T_i'(y) + a_5 \sum_{i=0}^{N} c_{3(N+1)+i} T_i'(y) = 0 \tag{3.108}$$

$$a_6 \sum_{i=0}^{N} c_i T_i(y) + \sum_{i=0}^{N} c_{N+1+i} T_i'(y) + a_6 \sum_{i=0}^{N} c_{2(N+1)+i} T_i(y) \tag{3.109}$$

$$-\mathrm{i}\omega \sum_{i=0}^{N} c_{3(N+1)+i} T_i(y) + a_7 \sum_{i=0}^{N} c_i T_i(y) + a_8 \sum_{i=0}^{N} c_{N+1+i} T_i'(y) + a_9 \sum_{i=0}^{N} c_{3(N+1)+i} T_i''(y) = 0 \tag{3.110}$$

The boundary conditions (3.16)–(3.22) are reduced to

$$-\frac{Q_{s0} r}{\beta \theta_n^{1/2}} \sum_{i=0}^{N} c_{3(N+1)+i} T_i'(-1) - \epsilon \frac{0.6 K \theta_n r S_R}{\beta} \sum_{i=0}^{N} c_i T_i(-1) = 0 \tag{3.111}$$

$$-\frac{Q_{s0} r}{\beta \theta_n^{1/2}} \sum_{i=0}^{N} c_{3(N+1)+i} T_i'(1) + \epsilon \frac{0.6 K \theta_n r S_R}{\beta} \sum_{i=0}^{N} c_i T_i(1) = 0 \tag{3.112}$$

$$-\frac{\omega}{k}\sum_{i=0}^{N} c_{N+1+i}T_i(-1)-\frac{\mathrm{i}\omega}{\beta S_R}\sum_{i=0}^{N} c_{3(N+1)+i}T_i(-1)+\epsilon\frac{0.6K\theta_n r S_R}{\beta}\sum_{i=0}^{N} c_i T_i(-1)=0 \tag{3.113}$$

$$-\frac{\omega}{k}\sum_{i=0}^{N} c_{N+1+i}T_i(1)+\frac{\mathrm{i}\omega}{\beta S_L}\sum_{i=0}^{N} c_{3(N+1)+i}T_i(1)-\epsilon\frac{0.6K\theta_n r S_L}{\beta}\sum_{i=0}^{N} c_i T_i(1)=0 \tag{3.114}$$

In the spectral collocation method, the governing equations (3.107)–(3.110) are evaulated at the following Gauss-Lobatto points:

$$y_i=\cos\frac{i\pi}{N} \tag{3.115}$$

When i changes from 0 to N, y_i is found to change from 1 to -1. We obtain $4\times(N+1)$ equations from (3.107)–(3.110) in the form

$$\begin{gathered}
a_1\sum_{i=0}^{N} c_iT_i(y_0)+a_2\sum_{i=0}^{N} c_{2(N+1)+i}T_i(y_0)+a_3\sum_{i=0}^{N} c_{3(N+1)+i}T_i(y_0)=0\\
a_1\sum_{i=0}^{N} c_iT_i(y_1)+a_2\sum_{i=0}^{N} c_{2(N+1)+i}T_i(y_1)+a_3\sum_{i=0}^{N} c_{3(N+1)+i}T_i(y_1)=0\\
\cdots\cdots\cdots\cdots\cdots\\
\cdots\cdots\cdots\cdots\cdots\\
\cdots\cdots\cdots\cdots\cdots\\
a_1\sum_{i=0}^{N} c_iT_i(y_N)+a_2\sum_{i=0}^{N} c_{2(N+1)+i}T_i(y_N)+a_3\sum_{i=0}^{N} c_{3(N+1)+i}T_i(y_N)=0\\
a_4\sum_{i=0}^{N} c_{N+1+i}T_i(y_0)+a_5\sum_{i=0}^{N} c_{2(N+1)+i}T_i'(y_0)+a_5\sum_{i=0}^{N} c_{3(N+1)+i}T_i'(y_0)=0\\
a_4\sum_{i=0}^{N} c_{N+1+i}T_i(y_1)+a_5\sum_{i=0}^{N} c_{2(N+1)+i}T_i'(y_1)+a_5\sum_{i=0}^{N} c_{3(N+1)+i}T_i'(y_1)=0\\
\cdots\cdots\cdots\cdots\cdots\\
\cdots\cdots\cdots\cdots\cdots\\
\cdots\cdots\cdots\cdots\cdots\\
a_4\sum_{i=0}^{N} c_{N+1+i}T_i(y_N)+a_5\sum_{i=0}^{N} c_{2(N+1)+i}T_i'(y_N)+a_5\sum_{i=0}^{N} c_{3(N+1)+i}T_i'(y_N)=0\\
a_6\sum_{i=0}^{N} c_iT_i(y_0)+\sum_{i=0}^{N} c_{N+1+i}T_i'(y_0)+a_6\sum_{i=0}^{N} c_{2(N+1)+i}T_i(y_0)\\
a_6\sum_{i=0}^{N} c_iT_i(y_1)+\sum_{i=0}^{N} c_{N+1+i}T_i'(y_1)+a_6\sum_{i=0}^{N} c_{2(N+1)+i}T_i(y_1)\\
\cdots\cdots\cdots\cdots\cdots\\
\cdots\cdots\cdots\cdots\cdots\\
\cdots\cdots\cdots\cdots\cdots\\
a_6\sum_{i=0}^{N} c_iT_i(y_N)+\sum_{i=0}^{N} c_{N+1+i}T_i'(y_N)+a_6\sum_{i=0}^{N} c_{2(N+1)+i}T_i(y_N)\\
-\mathrm{i}\omega\sum_{i=0}^{N} c_{3(N+1)+i}T_i(y_0)+\cdots+a_9\sum_{i=0}^{N} c_{3(N+1)+i}T_i''(y_0)=0\\
-\mathrm{i}\omega\sum_{i=0}^{N} c_{3(N+1)+i}T_i(y_1)+\cdots+a_9\sum_{i=0}^{N} c_{3(N+1)+i}T_i''(y_1)=0\\
\cdots\cdots\cdots\cdots\cdots\\
\cdots\cdots\cdots\cdots\cdots\\
\cdots\cdots\cdots\cdots\cdots\\
-\mathrm{i}\omega\sum_{i=0}^{N} c_{3(N+1)+i}T_i(y_N)+\cdots+a_9\sum_{i=0}^{N} c_{3(N+1)+i}T_i''(y_N)=0
\end{gathered} \tag{3.116}$$

Among the above equations, some of the equations evaluated at $y=y_0(y=1)$ and $y=y_N(y=-1)$ are replaced with the boundary conditions. Considering

the order of differentiation with respect to y of each equation, we drop the first equation of the momentum equation in the y direction, the last equation of the continuity equation, and the first and the last equations of the Exner equation, and use the boundary conditions instead. The $4\times(N+1)$ equations are then

$$
\begin{gathered}
-\frac{Q_{s0}r}{\beta\theta_n^{1/2}}\sum_{i=0}^{N} c_{3(N+1)+i}T_i'(-1) - \epsilon\frac{0.6K\theta_n r S_R}{\beta}\sum_{i=0}^{N} c_i T_i(-1) = 0 \\
-\frac{Q_{s0}r}{\beta\theta_n^{1/2}}\sum_{i=0}^{N} c_{3(N+1)+i}T_i'(1) + \epsilon\frac{0.6K\theta_n r S_R}{\beta}\sum_{i=0}^{N} c_i T_i(1) = 0 \\
-\frac{\omega}{k}\sum_{i=0}^{N} c_{N+1+i}T_i(-1) - \frac{\mathrm{i}\omega}{\beta S_R}\sum_{i=0}^{N} c_{3(N+1)+i}T_i(-1) + \epsilon\frac{0.6K\theta_n r S_R}{\beta}\sum_{i=0}^{N} c_i T_i(-1) = 0 \\
-\frac{\omega}{k}\sum_{i=0}^{N} c_{N+1+i}T_i(1) + \frac{\mathrm{i}\omega}{\beta S_L}\sum_{i=0}^{N} c_{3(N+1)+i}T_i(1) - \epsilon\frac{0.6K\theta_n r S_L}{\beta}\sum_{i=0}^{N} c_i T_i(1) = 0 \\
a_1\sum_{i=0}^{N} c_i T_i(y_0) + a_2\sum_{i=0}^{N} c_{2(N+1)+i}T_i(y_0) + a_3\sum_{i=0}^{N} c_{3(N+1)+i}T_i(y_0) = 0 \\
\cdots\cdots\cdots\cdots\cdots \\
\cdots\cdots\cdots\cdots\cdots \\
\cdots\cdots\cdots\cdots\cdots \\
a_1\sum_{i=0}^{N} c_i T_i(y_N) + a_2\sum_{i=0}^{N} c_{2(N+1)+i}T_i(y_N) + a_3\sum_{i=0}^{N} c_{3(N+1)+i}T_i(y_N) = 0 \\
a_4\sum_{i=0}^{N} c_{N+1+i}T_i(y_1) + a_5\sum_{i=0}^{N} c_{2(N+1)+i}T_i'(y_1) + a_5\sum_{i=0}^{N} c_{3(N+1)+i}T_i'(y_1) = 0 \\
\cdots\cdots\cdots\cdots\cdots \\
\cdots\cdots\cdots\cdots\cdots \\
\cdots\cdots\cdots\cdots\cdots \\
a_4\sum_{i=0}^{N} c_{N+1+i}T_i(y_N) + a_5\sum_{i=0}^{N} c_{2(N+1)+i}T_i'(y_N) + a_5\sum_{i=0}^{N} c_{3(N+1)+i}T_i'(y_N) = 0 \\
a_6\sum_{i=0}^{N} c_i T_i(y_0) + \sum_{i=0}^{N} c_{N+1+i}T_i'(y_0) + a_6\sum_{i=0}^{N} c_{2(N+1)+i}T_i(y_0) \\
\cdots\cdots\cdots\cdots\cdots \\
\cdots\cdots\cdots\cdots\cdots \\
\cdots\cdots\cdots\cdots\cdots \\
a_6\sum_{i=0}^{N} c_i T_i(y_{N-1}) + \sum_{i=0}^{N} c_{N+1+i}T_i'(y_{N-1}) + a_6\sum_{i=0}^{N} c_{2(N+1)+i}T_i(y_{N-1}) \\
-\mathrm{i}\omega\sum_{i=0}^{N} c_{3(N+1)+i}T_i(y_1) + \cdots + a_9\sum_{i=0}^{N} c_{3(N+1)+i}T_i''(y_1) = 0 \\
\cdots\cdots\cdots\cdots\cdots \\
\cdots\cdots\cdots\cdots\cdots \\
\cdots\cdots\cdots\cdots\cdots \\
-\mathrm{i}\omega\sum_{i=0}^{N} c_{3(N+1)+i}T_i(y_{N-1}) + \cdots + a_9\sum_{i=0}^{N} c_{3(N+1)+i}T_i''(y_{N-1}) = 0
\end{gathered}
\tag{3.117}
$$

The above equations can be rewritten in the following matrix form:

$$
\mathbf{L}\cdot\boldsymbol{c} = 0 \tag{3.118}
$$

where

$$\mathbf{L} = \begin{bmatrix} -\epsilon\frac{0.6K\theta_n r S_R}{\beta}T_0(-1) & -\epsilon\frac{0.6K\theta_n r S_R}{\beta}T_1(-1) & \cdots & -\frac{Q_{s0}r}{\beta\theta_n^{1/2}}T_N(-1) \\ \epsilon\frac{0.6K\theta_n r S_R}{\beta}T_0(1) & -\epsilon\frac{0.6K\theta_n r S_R}{\beta}T_1(1) & \cdots & -\frac{Q_{s0}r}{\beta\theta_n^{1/2}}T_N(1) \\ \epsilon\frac{0.6K\theta_n r S_R}{\beta}T_0(-1) & -\epsilon\frac{0.6K\theta_n r S_R}{\beta}T_1(-1) & \cdots & -\frac{\mathrm{i}\omega}{\beta S_R}T_N(-1) \\ \epsilon\frac{0.6K\theta_n r S_R}{\beta}T_0(1) & -\epsilon\frac{0.6K\theta_n r S_R}{\beta}T_1(1) & \cdots & -\frac{\mathrm{i}\omega}{\beta S_R}T_N(1) \\ a_1T_0(y_0) & a_1T_1(y_0) & \cdots & a_3T_N(y_0) \\ \cdot & \cdot & \cdots & \cdot \\ \cdot & \cdot & \cdots & \cdot \\ a_1T_0(y_N) & a_1T_1(y_N) & \cdots & a_3T_N(y_N) \\ 0 & 0 & \cdots & a_5T'_N(y_1) \\ \cdot & \cdot & \cdots & \cdot \\ \cdot & \cdot & \cdots & \cdot \\ 0 & 0 & \cdots & a_5T'_N(y_N) \\ a_6T_0(y_0) & a_6T_1(y_0) & \cdots & 0 \\ \cdot & \cdot & \cdots & \cdot \\ \cdot & \cdot & \cdots & \cdot \\ a_6T_0(y_{N-1}) & a_6T_1(y_{N-1}) & \cdots & 0 \\ a_7T_0(y_1) & a_7T_1(y_1) & \cdots & -\mathrm{i}\omega T_{N-1}(y_1) + a_9T''_{N-1}(y_1) \\ \cdot & \cdot & \cdots & \cdot \\ \cdot & \cdot & \cdots & \cdot \\ a_7T_0(y_{N-1}) & a_7T_1(y_{N-1}) & \cdots & -\mathrm{i}\omega T_{N-1}(y_{N-1}) + a_9T''_{N-1}(y_{N-1}) \end{bmatrix} \tag{3.119}$$

$$\boldsymbol{c} = \begin{bmatrix} c_0 \\ c_1 \\ \cdot \\ \cdot \\ c_N \\ c_{N+1} \\ \cdot \\ \cdot \\ c_{2N+1} \\ c_{2(N+1)} \\ \cdot \\ \cdot \\ c_{3N+2} \\ c_{3(N+1)} \\ \cdot \\ \cdot \\ c_{4N+3} \end{bmatrix} \tag{3.120}$$

In order for (3.118) to have non-trivial solution, the following condition has to be satisfied:

$$|\mathbf{L}| = 0 \tag{3.121}$$

Because $\mathbf{L}$ includes k, ω, β and other parameters such as the Froude number F, the Shields number θ_n, the bed Friction coefficient C_f, and the bank slopes S_R and S_L. We obtain the following relation:

$$\omega = f(k, \beta; F, \theta_n, C_f, S_R, S_L) \tag{3.122}$$

Chapter 4

Results and discussion

4.1 Analytical results

The analytical model accounts for the variability of the parameters to investigate the effect on both cases of pure bar instability and bar instability with bank erosion. The results obtained from linear stability analysis are presented herein. In the first subsection, the growth rates of perturbation Im[ω] are plotted in the dimensionless wavenumber - aspect ratio plane, or the k-β plane. In the second subsection, the values of Im[ω] are plotted against k, while in the last subsection, the spatial distribution of the unknown variables H_1, U_1, V_1, Z_1 and phase diagrams are presented. The flow and sediment parameters used in the theoretical analysis are as follows: K=7.6, r=0.5, F=0.5, C_f=0.010, θ_n=0.06, θ_c=0.05, S_R=S_L=1.0, and ϵ=1.0.

4.1.1 Instability diagrams in the k - β plane

In **Fig. 4.1** - **Fig. 4.10**, the dashed contours represent growth rates of perturbation or Im[ω] for pure bar instability, while the solid contours represent growth rates for bar instability with bank erosion. The contour for zero growth rate, or the neutral curve, refers to the case where the perturbation neither grows nor decays (e.g.Im[ω]=0). It is the curve that delineates the stable region (e.g.Im[ω]<0) and the unstable region (e.g.Im[ω]>0). In the stable region, the base state that is initiated as the flat bed is stable; on the other hand, in the unstable region, the pertubation grows, and it can be considered that in this region, bars initially develop. **Fig. 4.1** - **Fig. 4.4** report the variability of Froude number, with the bed friction coefficient C_f=0.01. It is observed that as the Froude number is increased from 0.2 to 1.2, the unstable region shifts to a range of smaller wavenumbers. The same observation can be derived for **Fig. 4.8** - **Fig. 4.10**, since the Froude number is

varied as well, but C_f is taken at 0.005. On the other hand, when the Shields number θ_n is increased from 0.06 to 0.10 as shown in **Fig. 4.5 - Fig. 4.7**, the critical aspect ratio increases from approximately 6.0 to approximately 9.0. The critical aspect ratio β_{cr} is the minimum value of the range of aspect ratios beyond which bars initially develop. As such, the threshold value of the aspect ratio increases with respect to an increase of Shields number. Furthermore, as the Shields number increases, the growth rate contours of bar instability with bank erosion coincides with that of pure bar instability. This indicates that the effect of bank erosion is significant at θ_n=0.06, and as it is maximized, the effect of bank erosion becomes less relevant. A look at Eq. (2.51) and Eq. (2.52) may provide the explanation. We assume that bank erosion occurs in both banks, such that Q_{sRj} is positive and Q_{sLj} is negative. Taking the right bank as an example, when θ_n increases, the terms (θ-θ_n)($\theta^{1/2}$-0.7$\theta_n^{1/2}$) decrease, such that the lateral sediment transport rate exchanged from the bank region to the bed region Q_{sRj} is minimized. Hence, the amount of sediment supplied from the bank to the bed is reduced for as long as θ_n is increased.

4.1.2 Plot of Im[ω] vls k: Variation of ϵ

When ϵ=0, bank erosion vanishes; when the value is 1, the banks are erodible such that there is no protection that inhibits bank erosion, either in the form of slump blocks or the presence of vegetation. As shown in **Fig. 4.11**, the value of ϵ is varied to clarify the effect of bank erosion. It is revealed that the unstable region shifts to a range of smaller wavenumbers when ϵ increases from 0 to 1. This indicates that when bank erosion is incorporated into the analysis, the wavelength of the bars are longer than when there is no bank erosion.

In linear theory, there exists a maximum growth rate of perturbation Im[ω_{max}] that corresponds to the dominant wavenumber. The dominant wavenumber, or k_{dom}, when converted into the wavelength as found in Eq. (4.1), is thought to be the representative wavelength from the theoretical analysis that serves as an estimate of the wavelength that is observed in the experiment [23]. The influence of the variability of ϵ on Im[ω_{max}] and the shift of wavenumbers are examined in **Fig. 4.12 - Fig. 4.19**. The horizontal axis denotes k, while the vertical axis denotes $Im[\omega]$. It is generally observed for the aforementioned figures that the maximum growth rates of perturbation tend to decrease considerably as ϵ increases; on the contrary, for **Fig. 4.12** and **Fig. 4.18**, the trend of the values of Im[ω_{max}] indicate otherwise. In addition, for **Fig. 4.12 - Fig. 4.19**, the contours shift to a range of smaller wavenumbers, which is opposite to **Fig. 4.18**. Meanwhile, for **Fig. 4.20**

- **Fig. 4.23**, the aspect ratio is varied with values β=10, 20, 30 and 40 for θ_n=0.08. It is shown that the maximum growth rates of perturbation are amplified with respect to an increase in aspect ratio. This confirms the influence of the aspect ratio as one of the governing parameters of bar instability; at high aspect ratios, bars are more likely to form, and multiple bars may exist. However, multiple bars are beyond the scope of this study. It is also worth mentioning that as β approaches 40, the contours for ϵ=0, 0.3, 0.7 and 1.0 overlap. Furthermore, as the aspect ratio increases, the contours shift to a range of larger wavenumbers, or smaller wavelength values. It is thought that at high aspect ratios, the effect of ϵ is significantly reduced. It is possible that when the width of the channel is relatively wide, the sidewall effects, such as the slumping of a portion of the bank to the bank toe or the presence of vegetation, are minimal.

4.1.3 Phase diagrams and spatial distribution of H_1, U_1, V_1, Z_1

In order to show how the perturbation progresses downstream, the spatial distribution diagrams illustrated in density plots of the variables H_1, U_1, V_1, Z_1 at β=10 are shown in **Fig. 4.26** - **Fig. 4.29**. The horizontal axis denotes the units of length in the streamwise direction, the lateral coordinate denotes length in the channel cross-section, in which y=1 denotes the left bank and y=-1 denotes the right bank. The vertical axis directed perpendicular and out of the figure are the numerical values of the variables. It is noted that the sinusoidal functions of both U_1 and Z_1 are in-phase, and both variables are out-of-phase with H_1. The variable V_1 is parabolic. The perturbation progresses downstream in a periodic manner. Furthermore, the phases are shown in **Fig. 4.24** - **Fig. 4.25**. It is found that for a given β=10, U_1 and Z_1 are in-phase, while V_1 and H_1 are also in phase with each other. The same relation can be observed for β=20. Finally, the phases of the variables R_1 and L_1 coincide, indicating that the banks are in-phase with each other.

4.2 Comparison of theoretical results with experimental results

The validation of the theoretical results from linear stability analysis is performed through a comparison of the theoretical bar wavelength values with experimental values obtained from studies of alternate bars. In addition, the computed maximum growth rates are obtained from the stability analysis following the flow and sediment characteristics employed in the experimental set-up. If the maximum growth rate is positive, bars are theoretically

formed; it is then verified into the experimental set-up if bars have indeed formed.

For the case of non-erodible banks, the results of Watanabe et al.[22] for steady flow conditions and of Lanzoni [23] for free bars are used. For the case of both erodible and non-erodible banks, the values are approximated from the work of Carrasco-Milian and Vionnet [8]. It is again worth mentioning here that theoretical results are based on the case with no bank erosion, and with bank erosion but no slump blocks (i.e. $\epsilon = 1$), since the experiments used sand. While the number of runs and experimental conditions for the experimental studies are not sufficient to provide reliable comparison of the theoretical results, only the general trend is considered herein.

The predicted wavelength is computed as

$$\lambda_c = \frac{2\pi \tilde{B_n}}{k_{dom}} \tag{4.1}$$

where λ_c is the computed wavelength, $\tilde{B_n}$ is the half-channel width at normal flow condition, and k_{dom} is the dominant wavenumber corresponding to maximum growth rate of perturbation from linear stability analysis.

Fig. 4.30 reports the the predicted values of bar wavelength plotted against the values of the observed wavelength. The theoretical values predicted by the analysis for [22] fall within 1.4m - 1.6m, and their obtained experimental values range within 2.0m - 3.4m. On the other hand, the theoretical values range from 5.5m - 6.7m, while the experimental values fall within 11.6m - 6m for [23]. It is revealed that the experimental values are twice as large as the calculated values of bar wavelength. However, for the case of [23], the agreement is relatively good as long as the experimental values fall within around 6m - 8m; at observed values higher than this range, the calculated values tend to underestimate the observed values of bar wavelength.

Meanwhile, as reflected on the results for [22], it is worth noting data points in **Fig. 4.30** where the observed wavelength is zero but the theoretical results record otherwise. Such is the case where no bars formed during the experimental runs. As shown in Table 4.1, no bars formed for runs S-5 to S-6. Yet, basing from the theoretical analysis, all of the six experimental conditions yielded an unstable condition. This means that using the flow and sediment parameters of the study, bars theoretically form in all of the experimental set-up, which is not the case for the experiment of [22], who noticed that alternate bars formed only when the flow depth is less than 2.5cm.

On the contrary, there is good agreement between the theoretical results with the experimental results of [23]. The maximum growth rates are posi-

tive, found in Table 4.3. In this case, based on the hydraulic conditions used in the experiment, the base state is unstable and allows for bars to initially form. As for the experiment, all of the 11 conditions were able to detect the growth of bars. It is possible that the favorable trend exhibited by the theoretical results when compared to the results of [23] is attributed to the high values of the aspect ratio, where the channel width is relatively wider than that of [22]. In addition to the aspect ratio, the Froude number and the bed friction coefficient are among the parameters that influence the growth rate, and hence the initial formation of bars.

Instability diagrams in the k-β plane provide a rough estimate of which range of aspect ratios will provide the region where bars initially develop, and the range of wavenumbers as well, under a given set of flow and sediment parameters. Hence, the results in an instability diagram may serve as guide for an experimental set-up. According to [5], the predicted meander wavelength is thought to provide a crude estimate of wavelengths observed in flume studies and field conditions. However, inerodible banks do not allow for meandering to develop; hence, for meandering to progress, banks must erode as well.Herein, the role of bank erosion to the formation of alternate bars is investigated. The results of the experiment of Carrasco-Milian and Vionnet [8] are used, particularly the values observed at the initial time of the experiment, or when the bars are starting to develop. It is to be noted, however, that data are approximated and do not reflect the actual values themselves.

The flow and sediment parameters are tabulated in Table4.2. The observed wavelength values for both cases of erodible and non-erodible banks are plotted with respect to the aspect ratio, as shown in **Fig. 4.31**. Wavelength values for non-erodible banks range from 0.6m - 3.7m, while the values of erodible banks range from 0.4m - 2.55m. Apparently, the results for the case of non-erodible banks are slightly larger than the case of erodible banks. However, this observation could not provide explanation for how bank erosion affects bar formation. Furthermore, as shown in **Fig. 4.32** and **Fig. 4.33**, the theoretical analysis predicts the base state of the experiment to be stable, for the case of erodible and non-erodible banks. The experimental results lie within the stable region, in which bars do not develop. The unstable region starts to initially develop at a critical aspect ratio $\beta_{cr} = 6.4$, whereas the experiment uses $\beta = 5.7$. This elaborates the role of the aspect ratio as a governing parameter for bars to initially develop. Hence, the theoretical results do not agree well with the experimental results.

According to Lanzoni [23], most theoretical results and flume studies usually are only valid for high values of aspect ratio, since the assumption is that the channel is relatively wide, or that the banks are not very steep. If

the banks are too steep, the sidewall effects may affect the flow in the central bed region. Such is the case of [8], where the bank slopes are both equal to 60 degrees. It is also worth noting that as found on Table 4.1 and 4.2, the Froude number F for both experiments is approximately equal to 0.7, which is quite high. For flume studies where the channel width ranges from 20 - 50cm and flow depth ranges from 1cm - 4cm, F usually ranges from 0.6 -0.7 [23]. On the contrary, for field data, the range is usually 0.2 - 0.3. Hence, it may also be interesting to consider bar wavelength values observed in field conditions.

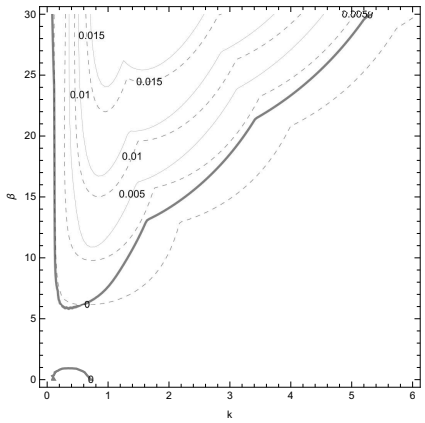

Figure 4.1: $K = 7.6$, $r = 0.5$, $S_B = 1$, $\theta_n = 0.06$, $\theta_c = 0.05$, $C_f = 0.010$, $F = 0.5$, $\epsilon = 1$, Dashed contours: pure bar instability, Solid contours: bar instability with bank erosion.

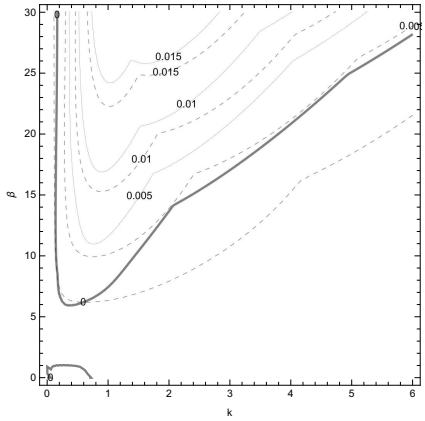

Figure 4.2: $K = 7.6$, $r = 0.5$, $S_B = 1$, $\theta_n = 0.06$, $\theta_c = 0.05$, $C_f = 0.010$, $F = 0.2$, $\epsilon = 1$, Dashed contours: pure bar instability, Solid contours: bar instability with bank erosion.

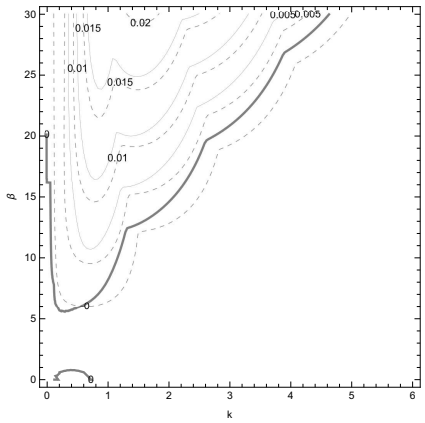

Figure 4.3: $K = 7.6$, $r = 0.5$, $S_B = 1$, $\theta_n = 0.06$, $\theta_c = 0.05$, $C_f = 0.010$, $F = 0.8$, $\epsilon = 1$, Dashed contours: pure bar instability, Solid contours: bar instability with bank erosion.

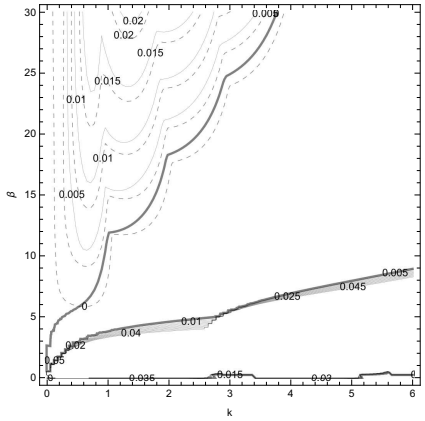

Figure 4.4: $K = 7.6$, $r = 0.5$, $S_B = 1$, $\theta_n = 0.06$, $\theta_c = 0.05$, $C_f = 0.010$, $F = 1.2$, $\epsilon = 1$, Dashed contours: pure bar instability, Solid contours: bar instability with bank erosion.

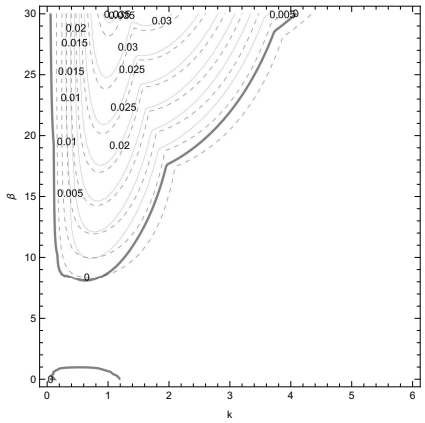

Figure 4.5: $K = 7.6$, $r = 0.5$, $S_B = 1$, $\theta_n = 0.08$, $\theta_c = 0.05$, $C_f = 0.010$, $F = 0.5$, $\epsilon = 1$, Dashed contours: pure bar instability, Solid contours: bar instability with bank erosion.

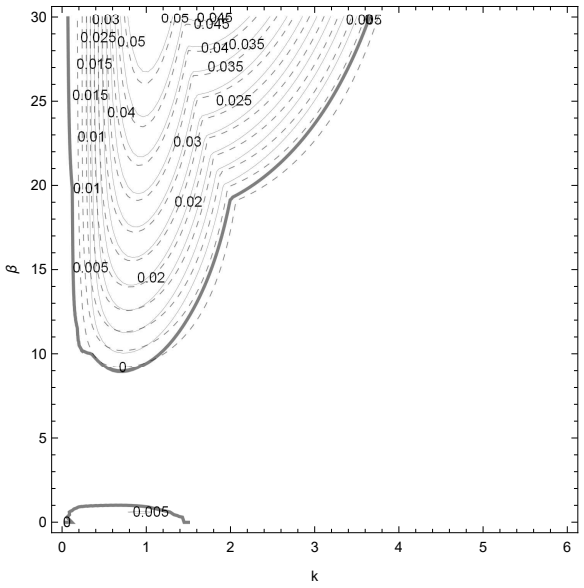

Figure 4.6: $K = 7.6$, $r = 0.5$, $S_B = 1$, $\theta_n = 0.10$, $\theta_c = 0.05$, $C_f = 0.010$, $F = 0.5$, $\epsilon = 1$, Dashed contours: pure bar instability, Solid contours: bar instability with bank erosion.

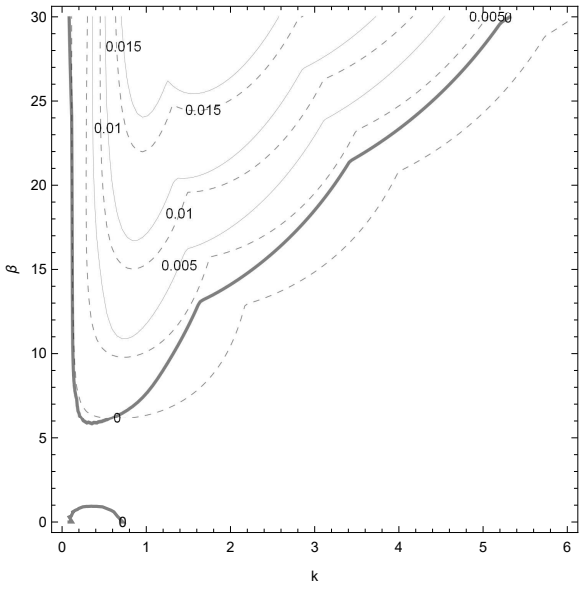

Figure 4.7: $K = 7.6$, $r = 0.5$, $S_B = 1$, $\theta_n = 0.06$, $\theta_c = 0.05$, $C_f = 0.010$, $F = 0.5$, $\epsilon = 1$, Dashed contours: pure bar instability, Solid contours: bar instability with bank erosion.

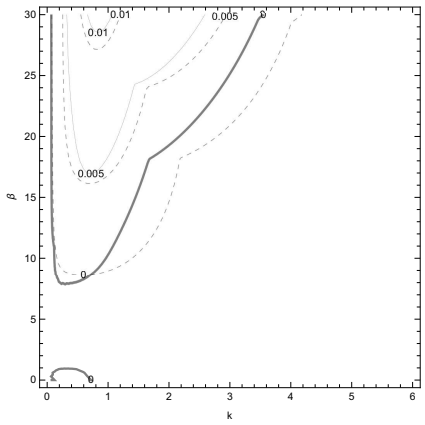

Figure 4.8: $K = 7.6$, $r = 0.5$, $S_B = 1$, $\theta_n = 0.06$, $\theta_c = 0.05$, $C_f = 0.005$, $F = 0.5$, $\epsilon = 1$, Dashed contours: pure bar instability, Solid contours: bar instability with bank erosion.

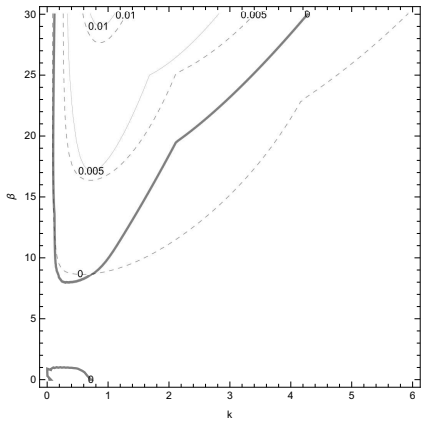

Figure 4.9: $K = 7.6$, $r = 0.5$, $S_B = 1$, $\theta_n = 0.06$, $\theta_c = 0.05$, $C_f = 0.005$, $F = 0.2$, $\epsilon = 1$, Dashed contours: pure bar instability, Solid contours: bar instability with bank erosion.

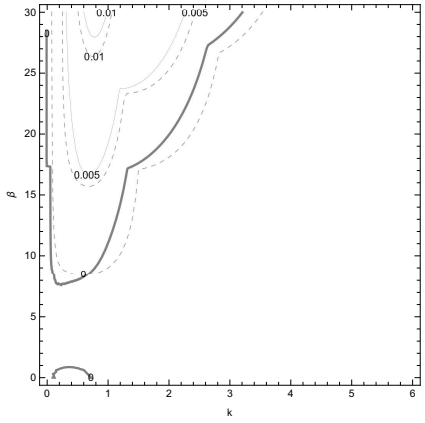

Figure 4.10: $K = 7.6$, $r = 0.5$, $S_B = 1$, $\theta_n = 0.06$, $\theta_c = 0.05$, $C_f = 0.005$, $F = 0.8$, $\epsilon = 1$, Dashed contours: pure bar instability, Solid contours: bar instability with bank erosion.

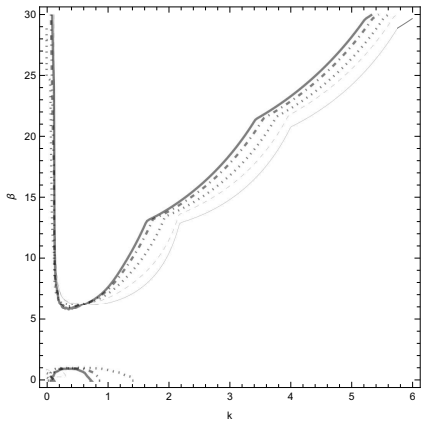

Figure 4.11: K=7.6, r=0.5, S_B=1, θ_n=0.06, θ_c=0.05, C_f=0.010, F=0.5, Thin solid contour: pure bar instability, from outside to inside: ϵ=0, 0.3, 0.7, 1, only neutral curves are shown.

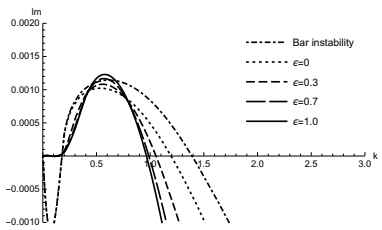

Figure 4.12: Plot for C_f=0.005, β=10

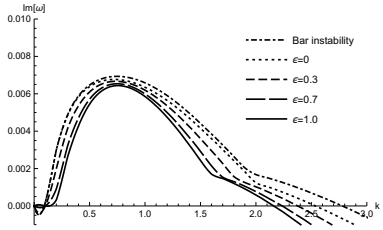

Figure 4.13: Plot for C_f=0.005, β=20

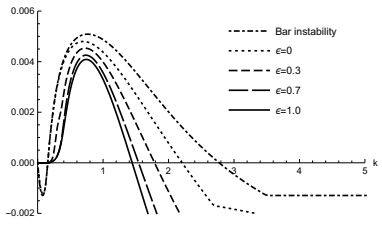

Figure 4.14: Plot for F=0.2, β=10

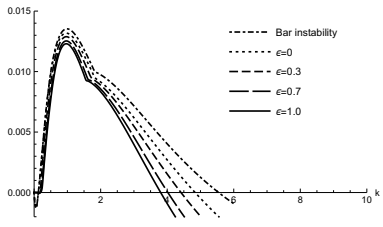

Figure 4.15: Plot for F=0.2, β=20

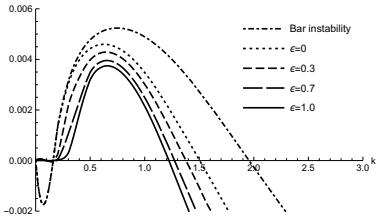

Figure 4.16: Plot for S_B=0.5, β=10

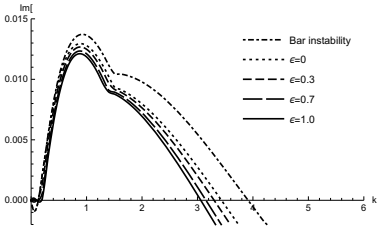

Figure 4.17: Plot for S_B=0.5, β=20

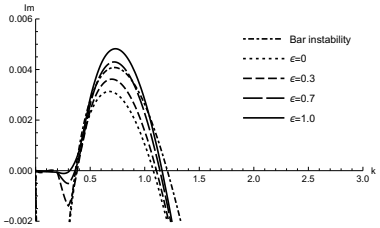

Figure 4.18: Plot for θ_n=0.1, β=10

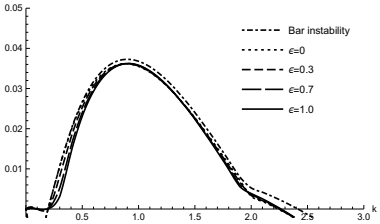

Figure 4.19: Plot for θ_n=0.1, β=20

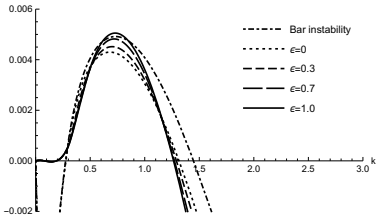

Figure 4.20: Plot for θ_n=0.08, β=10

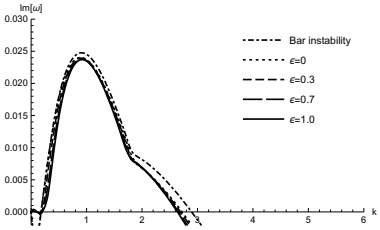

Figure 4.21: Plot for θ_n=0.08, β=20

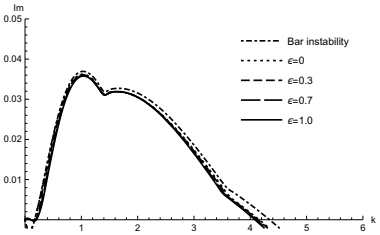

Figure 4.22: Plot for θ_n=0.08, β=30

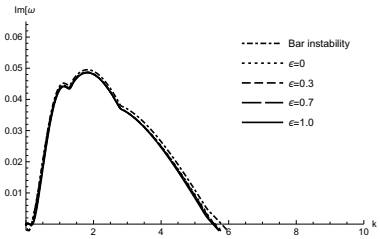

Figure 4.23: Plot for θ_n=0.08, β=40

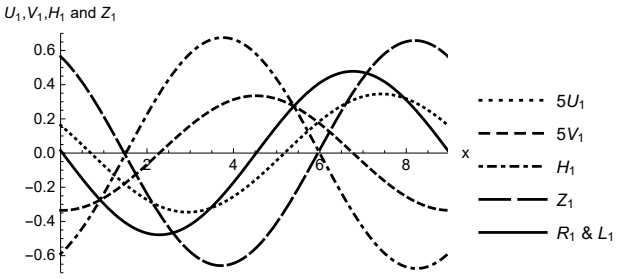

Figure 4.24: Plot for Z_1. $\beta = 10$.

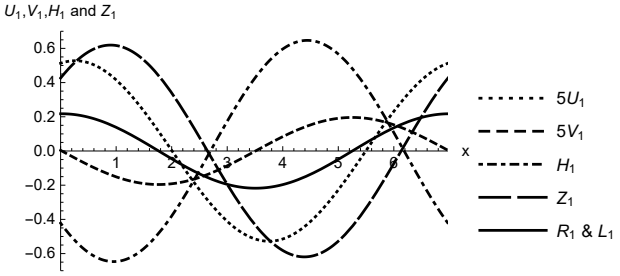

Figure 4.25: Plot for Z_1. $\beta = 20$.

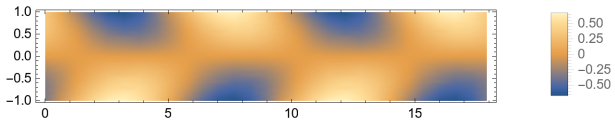

Figure 4.26: Plot for H_1. $\beta = 10$.

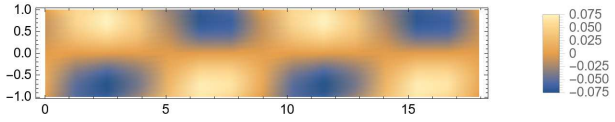

Figure 4.27: Plot for U_1. $\beta = 10$.

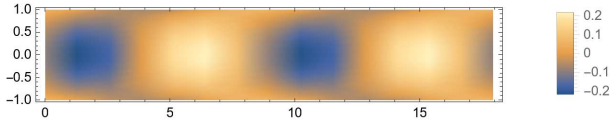

Figure 4.28: Plot for V_1. $\beta = 10$.

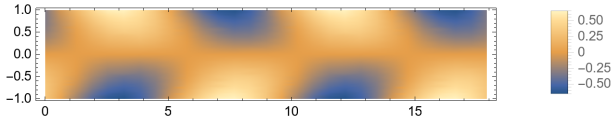

Figure 4.29: Plot for Z_1. $\beta = 10$.

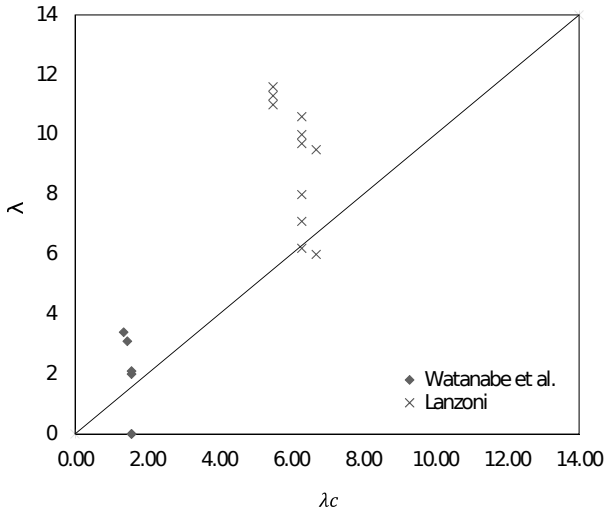

Figure 4.30: Test of our analysis with experimental data, where λ is the observed bar wavelength and λ_c in the x-axis is the calculated bar wavelength. Units in meters.

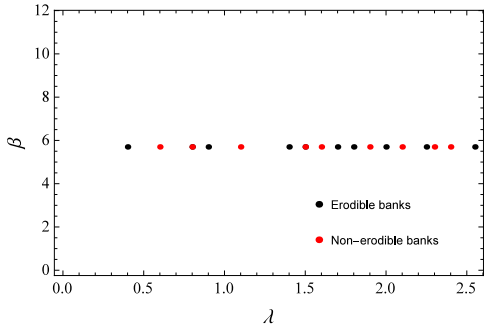

Figure 4.31: Approximated values of bar wavelength in meters, observed by Carrasco-Milian and Vionnet.

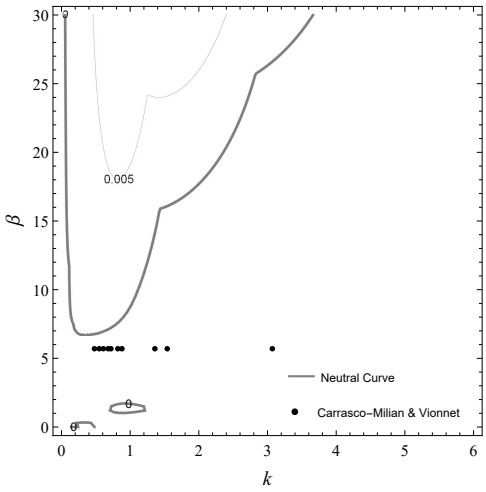

Figure 4.32: Plot of Carrasco-Milian and Vionnet's results in the instability diagram with bank erosion.

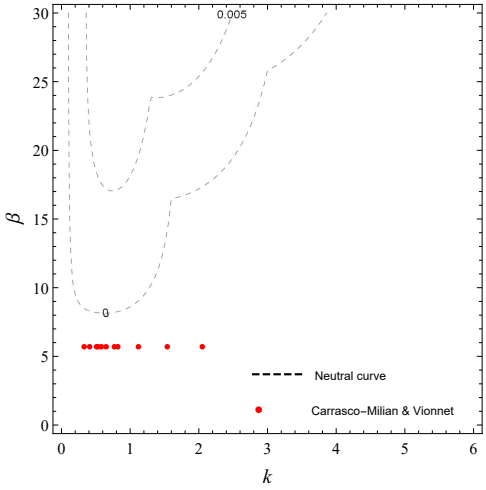

Figure 4.33: Plot of Carrasco-Milian and Vionnet's results in the instability diagram without bank erosion.

Table 4.1: Data from Watanabe et al.'s experiment for steady flow, including maximum growth rate

Run	Q_0, cm^3/s	$\tilde{B_n}$, m	S_{bed}	L_{bed}, m	$\tilde{d_s}$, mm	F	$\tilde{H_n}$, cm	C_f	θ_n	β	z_{bh}, cm	λ, m	$Im[\omega_{max}]$
S-1	750	0.30	0.006	50	0.76	0.775	1.02	0.0093	0.045	14.7	3.4	3.4	0.007
S-2	1320	0.30	0.006	50	0.76	0.772	1.49	0.0093	0.066	10.1	2.1	3.1	0.008
S-3	1990	0.30	0.006	50	0.76	0.778	1.95	0.0092	0.086	7.7	2.5	2.0	0.007
S-4	2500	0.30	0.006	50	0.76	0.753	2.32	0.0098	0.103	6.5	2.5	2.1	0.008
S-5	3070	0.30	0.006	50	0.76	0.753	2.66	0.0098	0.118	5.6	0	0	0.006
S-6	3470	0.30	0.006	50	0.76	0.740	2.92	0.0101	0.129	5.1	0	0	0.006

Table 4.2: Data from Carrasco-Milian and Vionnet's experiment

Q_0, cm^3/s	$\tilde{B_n}$, m	S_{bed}	L_{bed}, m	$\tilde{d_s}$, mm	F	$\tilde{H_n}$, cm	C_f	θ_n	θ_c	β	$S_R = S_L$
6000	0.391	0.002	22	0.94	0.733	3.43	0.00724	0.044	0.036	5.7	1.7

Notation are as follows: Q_0: flow discharge; $\tilde{B_n}$,: channel bottom width; S_{bed}: channel slope; L_{bed}: channel length; $\tilde{d_s}$: mean sediment diameter; F: Froude number; $\tilde{H_n}$: flow depth at normal flow; C_f: friction coefficient; θ_n: dnon-dimensional bed shear stress; β: ratio of half-channel width to flow depth; z_{bh}: bar height; λ : observed bar wavelength; $Im[\omega_{max}]$: maximum growth rate; S_R: right bank slope; S_L: left bank slope.

Table 4.3: Data from Lanzoni's experiment for free bars, including maximum growth rate

Run	Q_0, cm^3/s	$\tilde{B_n}$, m	i_s,%	L_{bed}, m	$\tilde{d_s}$, mm	F	$\tilde{H_n}$, cm	C_f	θ_n	β	z_{bh}, cm	λ, m	$Im[\omega_{max}]$
P801	30000	1.5	0.162	55	0.48	0.3191	7.3	0.0149	0.144	10.3	8.5	11.3	0.042
P2102	30000	1.5	0.162	55	0.48	0.3191	7.3	0.0149	0.144	10.3	4.0	11.6	0.042
P2403	47000	1.5	0.205	55	0.48	0.4211	8.3	0.0111	0.204	9.0	5.0-6.0	4.5-7.5	0.047
P0404	40000	1.5	0.201	55	0.48	0.4027	7.7	0.0121	0.187	9.7	6.0	4.3-8.0	0.049
P1204	40000	1.5	0.201	55	0.48	0.4080	7.5	0.0112	0.182	10.0	5.0	4.5-9.6	0.045
P2804	40000	1.5	0.201	55	0.48	0.4080	7.5	0.0112	0.182	10.0	5.0	8.0	0.045
P1505	30000	1.5	0.452	55	0.48	0.6849	4.4	0.0091	0.242	17.0	7.0	10.0	0.102
P1605	20000	1.5	0.495	55	0.48	0.7030	3.3	0.0095	0.201	22.7	7.7	11.0	0.102
P2709	45000	1.5	0.514	55	0.48	0.7088	5.7	0.01	0.356	13.2	4.5	9.7	0.158
P2809	40000	1.5	0.517	55	0.48	0.6934	5.3	0.0102	0.334	14.2	4.7	10.6	0.156
P2909	45000	1.5	0.516	55	0.48	0.7151	5.6	0.0096	0.352	13.4	4.4	9.8	0.152

Notation are as follows: Q_0: flow discharge; $\tilde{B_n}$,: channel bottom width; i_s: water surface slope; L_{bed}: channel length; $\tilde{d_s}$: mean sediment diameter; F: Froude number; $\tilde{H_n}$: flow depth at normal flow; C_f: friction coefficient; θ_n: dnon-dimensional bed shear stress; β: ratio of half-channel width to flow depth; z_{bh}: bar height; λ : observed bar wavelength; $Im[\omega_{max}]$: maximum growth rate.

Chapter 5

Conclusion

The study was able to perform linear stability analysis of the initial development of bars employing the shallow water equations, Exner equation, bedload transport models and a process-based bank erosion model. The analytical model accounts for the variability of the parameters such as the aspect ratio, Froude number, bed friction coefficient and bank slopes to investigate the influence to the instability of bars. It is found that bars are more likely to develop at low aspect ratios when the bed friction coefficient is increased. The study also reveals that the unstable region tends to shift to a range of smaller wavenumbers when the Froude number is maximized. Furthermore, the maximum growth rates of perturbation are amplified when the aspect ratio is increased; the same trend is exhibited by the growth rates when the bank slopes are increased.

In order to clarify the effect of bank erosion, the analytical model considered a parameter ϵ that inhibits bank erosion, such as slump block armouring coefficient or the presence of vegetation. It is revealed from the analysis that the theoretical wavelength of bars tend to become longer when ϵ is maximized. A similar observation can be obtained when the Shields number θ_n is varied, such that at $\theta_n = 0.06$, bank erosion is significant and at higher values, bank erosion is less relevant. It is possible that the net amount of sediment supplied from the banks undergoing erosion is reduced with respect to a decrease in either ϵ or θ_n.

Meanwhile, the flow and sediment parameters of the study of Carrasco-Milian and Vionnet were used to generate instability diagrams and the wavenumbers computed from the experiment were plotted. It is observed that the experimental data lie within the stable region where bars are not suppose to grow. The data does not exhibit a good agreement with the theoretical results. It is suggested that the aspect ratio be increased, such that the channel width is widened, in order to yield comparable results from stability

analysis.

Lastly, the study was also able to calculate values of the representative wavelength that were derived from the dominant wavenumbers corresponding to the maximum growth rates of perturbation. The flow and sediment parameters from the experimental studies of Watanabe et al. and Lanzoni for non-erodible banks were selected to obtain the representative or calculated wavelength, and were then compared with the experimental results. It is revealed that the calculated wavelength generally underestimates the observed wavelength, or the observed wavelength is twice as large as the calculated wavelength. It is possible that in the scheme of linear stability analysis, the instability process first selects the wavenumber and then enhances the growth rates of the bars; hence, bar formation in the stability analysis is slow.

Bibliography

[1] Norihiro Izumi: *Sediment transport* [Class handout], Division of Field Engineering for the Environment, Hokkaido University, Sapporo, Japan, 2016.

[2] Friedkin, J.F.: *A laboratory study of the meandering of alluvial rivers* (Googlebooks version), 1954. Available online: https://www.worldcat.org/title/laboratory-study-of-the-meandering-of- alluvial-rivers/oclc/758365105.

[3] Ryosaku Kinoshita: On the formation of sand bars in river channels –Observation of meandering channels–, Proceedings of JSCE, 42, 1–21, 1957.

[4] Eekhout, J. P. C., Hoitink, A. J. F., and Mosselman, E. : Field experiment on alternate bar development in a straight sand-bed stream, *Water Resour. Res*, 49, 8357-8369, 2013. doi: 10.1002/2013WR014259.

[5] Ikeda, S., G. Parker, and K. Sawai: Bend theory of river meanders, part 1, Linear development, *J. Fluid Mech.*, 112, 363-377, 1981.

[6] Tubino, M., and G. Seminara: Free-forced interactions in developing meanders and suppression of free bars, *J. Fluid Mech.*, 214, 131-159, 1990.

[7] Johanneson, H. and G. Parker: Linear theory of river meanders, In: *River Meandering* (Eds. S. Ikeda and G. Parker), pp. 181–213, AGU, 1989.

[8] Carrasco-Milian, A. and C. A. Vionnet: Experimental study on the formation of alternate bars with fixed and loose banks, *RCEM 2009 Proceedings, Argentina*, 773-778, 2010.

[9] Callander, R.A. : Instability and river channels, *J. Fluid Mech.*, 36, 465-480, 1969.

[10] Colombini, M., Seminara, G., and Tubino, M.: Finite amplitude alternate bars, *J. Fluid. Mech.*, 181, 213-232, 1987. doi: 10.1017/S002211087002064

[11] Shimada, R. et al.: Linear stability analysis on the meander formation originated by alternate bars, *JSCE Journal of Hydraulic Engineering*, 69(4), I1147-I1152 (in Japanese), 2013. doi: 10.2208/ jscejhe.69.I1147.

[12] Iwasaki, T., Shimizu, Y., and Kimura, I.: Sensitivity of free bar morphology in rivers to secondary flow modelling: Linear stability analysis and numerical simulation, *Advances in Water Resources*, 92, 57-72, 2016. doi: 10.2016/j.advwatres.2016.03.11.

[13] Uddin, M. J. et al. : Quasi-meandering induced by fluvial sandbars, *JSCE Journal of Hydraulic Engineering*, 71(4), I1021-I1026, (in Japanese), 2015. doi: 10.2208/jscejhe.71.I1021.

[14] Parker, G., Y. Shimizu, G. V. Wilerson, E. C. Eke, J. D. Abad, J. W. Lauer, C. Paola, W. E. Dietrich and V. R. Voller: A new framework for modeling the migration of meandering rivers, *Earth Surf. Process. Landforms*, 36, 70-86, 2011.

[15] Fujita, Y. and Y. Muramoto: Studies on the process of development of alternate bars, *Bulletin of the Disaster Prevention Research Institute*, 35(3), 55-86, 1985.

[16] Ryosaku Kinoshita: Investigation of the channel evolution of the Ishikari river, Natural Resources Bureau, Science and Technology Agency, 36, 1961.

[17] Hasegawa, K.: Universal Bank Erosion Coefficient for Meandering Rivers, *J. Hydraul. Eng.*, 115(6), 744-765, 1989.

[18] Parker, G., G. Seminara and L. Solari: Bed load at low Shields stress on arbitrarily sloping beds: Alternative entrainment formulation, *Water Resour. Res.*, 39(7), 1183, doi:10.1029/2001WR001253, 2003.

[19] Parker, G.: Self-formed straight rivers with equilibrium banks and mobile bed. 2: The gravel rivers, *Jour. Fluid Mech.*, 89, 127-146, 1978.

[20] Ikeda, S. and N. Izumi: Width and depth of self-formed straight gravel rivers with bank vegetation, *Water Resour. Res.*, 26(10), 2353-2364, 1990.

[21] Uddin, M. J., N. Izumi, K. Hasegawa and Y. Watanabe: Bar instability with bank erosion, Journal of JSCE, B1, 71(4), tentatively accepted.

[22] Watanabe, Y., M. Tubino, G. Zolezzi and K. Hoshi: Behavior of alternate bars under unsteady flow conditions, Available online: http://river.ceri.go.jp/contents/archive/docs/h13-303-312.pdf.

[23] Lanzoni, S.: Experiments on bar formation in a straight flume 1. Uniform sediment, *Water Resour. Res.*, 36(11), 3337-3349, 2000.

[24] Ikeda, S. and N. Izumi: Width and depth of self-formed straight gravel rivers with bank vegetation, *Water Resour. Res.*, 26(10), 2353-2364, 1990.